A&A 640, A2 (2020)
https://doi.org/10.1051/0004-6361/202038012

Astronomy & Astrophysics

Precise calibration of the dependence of surface brightness–colour relations on colour and class for late-type stars⋆,⋆⋆

A. Salsi[1], N. Nardetto[1], D. Mourard[1], O. Creevey[1], D. Huber[2], T. R. White[3,4,5], V. Hocdé[1], F. Morand[1], I. Tallon-Bosc[6], C. D. Farrington[7], A. Chelli[1], and G. Duvert[8]

[1] Université Côte d'Azur, OCA, CNRS Laboratoire, Lagrange, France
e-mail: anthony.salsi@oca.eu
[2] Institute for Astronomy, University of Hawaii, 2680 Woodlawn Drive, Honolulu, HI 96822, USA
[3] Sydney Institute for Astronomy, School of Physics A28, The University of Sydney, Sydney, NSW 2006, Australia
[4] Stellar Astrophysics Centre, Department of Physics and Astronomy, Aarhus University, 8000 Aarhus C, Denmark
[5] Research School of Astronomy and Astrophysics, Mount Stromlo Observatory, The Australian National University, Canberra, ACT 2611, Australia
[6] Univ. Lyon, Univ. Lyon 1, ENS de Lyon, CNRS, Centre de Recherche Astrophysique de Lyon UMR5574, 69230 Saint-Genis-Laval, France
[7] The CHARA Array, Mount Wilson Observatory, Mount Wilson, CA 91023, USA
[8] Univ. Grenoble Alpes, CNRS, IPAG, 38000 Grenoble, France

Received 24 March 2020 / Accepted 25 May 2020

ABSTRACT

Context. Surface brightness–colour relations (SBCRs) are used to derive the stellar angular diameters from photometric observations. They have various astrophysical applications, such as the distance determination of eclipsing binaries or the determination of exoplanet parameters. However, strong discrepancies between the SBCRs still exist in the literature, in particular for early and late-type stars.
Aims. We aim to calibrate new SBCRs as a function of the spectral type and the luminosity class of the stars. Our goal is also to apply homogeneous criteria to the selection of the reference stars and in view of compiling an exhaustive and up-to-date list of interferometric late-type targets.
Methods. We implemented criteria to select measurements in the JMMC Measured Diameters Catalog. We then applied additional criteria on the photometric measurements used to build the SBCRs, together with stellar characteristics diagnostics.
Results. We built SBCRs for F5/K7–II/III, F5/K7–IV/V, M–II/III and M–V stars, with respective rms of σ_{F_V} = 0.0022 mag, σ_{F_V} = 0.0044 mag, σ_{F_V} = 0.0046 mag, and σ_{F_V} = 0.0038 mag. This results in a precision on the angular diameter of 1.0%, 2.0%, 2.1%, and 1.7%, respectively. These relations cover a large $V-K$ colour range of magnitude, from 1 to 7.5. Our work demonstrates that SBCRs are significantly dependent on the spectral type and the luminosity class of the star. Through a new set of interferometric measurements, we demonstrate the critical importance of the selection criteria proposed for the calibration of SBCR. Finally, using the *Gaia* photometry for our samples, we obtained ($G-K$) SBCRs with a precision on the angular diameter between 1.1% and 2.4%.
Conclusions. By adopting a refined and homogeneous methodology, we show that the spectral type and the class of the star should be considered when applying an SBCR. This is particularly important in the context of PLATO.

Key words. techniques: interferometric – stars: atmospheres – stars: late-type – stars: fundamental parameters

1. Introduction

Surface brightness–colour relations (SBCRs) are very convenient tools for easily estimating the angular diameter of a star from photometric measurements. For instance, the SBCR plays a central role in the distance determination of eclipsing binaries, by combining the linear diameter (derived from light curve and velocimetry) and the estimated angular diameter of their components.

Recently, in the course of the Araucaria project (Pietrzyński & Gieren 2002), Pietrzyński et al. (2019) used this method to constrain the Large Magellanic Cloud distance to 1%. The PLATO (PLAnetary Transits and Oscillations of stars, Catala & PLATO Team 2006) space mission, planned for launch in 2026, will characterise exoplanetary systems, with the transit method. PLATO will thus provide the ratio of stellar-to-planet radii with 1% precision, while an SBCR combined with *Gaia* parallaxes will give access to the stellar radius.

So far, 23 SBCRs have been established, covering all spectral types and luminosity classes. Nardetto (2018) compares these SBCRs, and shows that they are precise but inconsistent for late-type stars (at the 10% level), while they are rather imprecise for early-type stars (around 7% precision, Challouf et al. 2014). Besides this, several studies, such as Fouque & Gieren (1997) and Kervella et al. (2004a) point out a significant difference in the SBCRs according to the luminosity class of the stars (see also, Nardetto 2018). They also suggest the impact of the activity of the star. Chelli et al. (2016) also proposed a different method based on so-called pseudo-magnitudes to build the JSDC catalogue, including 450 K star diameters.

⋆ Tables C.1–C.4 are only available at the CDS via anonymous ftp to cdsarc.u-strasbg.fr (130.79.128.5) or via http://cdsarc.u-strasbg.fr/viz-bin/cat/J/A+A/640/A2
⋆⋆ Based on CHARA/VEGA observations.

In the present work, we restrict our analysis to late-type stars, following the PLATO specifications, taking into account the luminosity classes as suggested by previous studies mentioned above. We only consider stars from F5 to K7, which corresponds to an effective temperature ($T_{\rm eff}$) lower than 6510 K (Pecaut & Mamajek 2013) (or $V-K \geq 1$ mag) and higher than 4050 K. We also consider $\log g = 4.0$ as the typical separation between dwarfs (V), sub-giants (IV) on one side, and giants (III) on the other side. This leads to four working samples; F5/K7 giants, F5/K7 sub-giants and dwarfs (II/III and IV/V luminosity classes, respectively), M giants, and M sub-giants and dwarfs.

We first present the SBCRs existing in the literature in Sect. 2. We then describe the selection of our interferometric and photometric measurements in Sect. 3, as well as the reddening law we used to correct the interstellar extinction. Our calibrated SBCRs are presented in Sect. 4 and discussed in Sect. 5.

2. Definition and surface brightness–colour relations in the literature

The surface brightness of a star is the flux density emitted per unit angular area. The Stefan-Boltzmann law connects the surface brightness to the effective temperature $T_{\rm eff}$. An empirical relation between the effective temperature and the colour (i.e. the difference in magnitude measured in two different spectral bands) of the star is then found to relate the surface brightness to the colour. The first historical definition of the surface brightness was established by Wesselink (1969), depending on the bolometric correction and the effective temperature of the star. Wesselink (1969) then used this definition to show the correlation between the surface brightness and the colour of the star. Later, Barnes & Evans (1976) built another definition of the surface brightness, noted F_λ, written as follows:

$$F_\lambda = C - 0.1 m_{\lambda_0} - 0.5 \log \theta_{\rm LD}, \quad (1)$$

where $\theta_{\rm LD}$ is the limb-darkened angular diameter of the star, m_{λ_0} is the apparent magnitude corrected from the interstellar extinction, and C is a constant. After Fouque & Gieren (1997), C depends on the Sun bolometric magnitude $M_{\rm bol_\odot}$, its total flux $f_\odot$, and the Stefan-Boltzmann constant σ through the following relationship (Fouque & Gieren 1997):

$$C = 0.1 M_{\rm bol_\odot} + 1 + 0.25 \log \frac{4 f_\odot}{\sigma}, \quad (2)$$

and it is found to be equal to 4.2207. More recent and accurate estimations of solar parameters (Mamajek et al. 2015; Prša et al. 2016) lead to a slightly different value, 4.2196, which we took for our study. The definition of the surface brightness can be rewritten as follows:

$$F_\lambda = 4.2196 - 0.1 m_{\lambda_0} - 0.5 \log \theta_{\rm LD}. \quad (3)$$

On the other hand, the bolometric surface flux $f_{\rm bol}$ of a star, which is expressed as the ratio between the bolometric flux $F_{\rm bol}$ and the squared limb-darkened angular diameter $\theta^2_{\rm LD}$, is linearly proportional to its effective temperature $T^4_{\rm eff}$. It is thus also linearly linked to the colour $m_{\lambda_1} - m_{\lambda_2}$. In this way, the surface brightness can be estimated by the following linear relation:

$$F_{\lambda_1} = a\,(m_{\lambda_1} - m_{\lambda_2}) + b. \quad (4)$$

The previous equation corresponds to the so-called surface brightness–colour relation (SBCR). By injecting Eq. (3) into Eq. (4), the SBCR allows us to directly estimate the limb-darkened angular diameter of the star. We used this definition of the SBCR in this work. Nardetto (2018) demonstrated the existence of various definitions of the SBCR in the literature. By carrying out suitable conversions, we compare the 23 SBCRs in Fig. 1, as a function of the $V-K$ colour. In the following, we consider the (V, $V-K$) colour system, as it is known to provide the lowest dispersion in the SBCRs (Kervella et al. 2004a). As shown by the figure, the SBCRs in the literature are rather consistent around $V-K = 2$ mag, with an expected precision on the derived angular diameter (using any SBCR) of about 2%. However, some discrepancies are clear on the outer edges of the surface brightness versus $V-K$ colour diagram, as already mentioned. In order to calibrate the SBCRs, we need the V and K magnitudes, the limb-darkened angular diameter, an extinction law, as well as diagnostics on star activity. We describe the strategy we implemented to find such information in the next subsections.

3. Methodology and selection criteria

The quality and robustness of an SBCR is strongly related to the definition of the samples of stars used for its calibration and to the correct explanation of its domain of validity. In this section, we present the method employed to define our samples on the basis of the JMMC Measured Diameters Catalog (JMDC) catalogue, and we detail the various selection criteria that were developed.

3.1. JMDC catalogue

The most complete and up-to-date catalogue that lists all the interferometric measurements that have been done so far is the JMMC Measured stellar Diameters Catalog[1] (Duvert 2016). As of February 2020, this catalogue contains 1672 rows. Among all these measurements, the current number of individual stars with observed diameters is 885. The catalogue lists the uniform disc angular diameter $\theta_{\rm UD}$, the limb-darkened angular diameter $\theta_{\rm LD}$, and the $\theta_{\rm UD}$ to $\theta_{\rm LD}$ conversion factor μ_λ if available. A "Notes" column is included and contains some information about the star. The observing technique is indicated: optical interferometry, lunar occultation or intensity interferometry. We cross-matched the *Simbad* database with the JMDC catalogue to obtain photometric information (see Sect. 3.5).

3.2. Common criteria

To build SBCRs, one needs several input data; $\theta_{\rm LD}$, $\sigma_{\theta_{\rm LD}}$, V, σ_V, K, and σ_K. We list the general criteria applied to our samples: (i) consider the spectral type (later than F5) and the luminosity class (II, III, IV or V) of the star; (ii) retain only optical interferometry measurements; (iii) reject measurements without all the necessary data ($\theta_{\rm LD}$, $\sigma_{\theta_{\rm LD}}$, V, σ_V, K and σ_K).

3.3. Stellar characteristics criteria

We implemented six more criteria based on the characteristics of the star. These criteria are presented in the top part of Table 1, with their corresponding labels used in the final table. When a star has one of these activity signs, it is not used to constrain the SBCRs, but it still appears in our final table of parameters.

[1] Available on the VizieR database at https://vizier.u-strasbg.fr/viz-bin/VizieR?-source=II/345

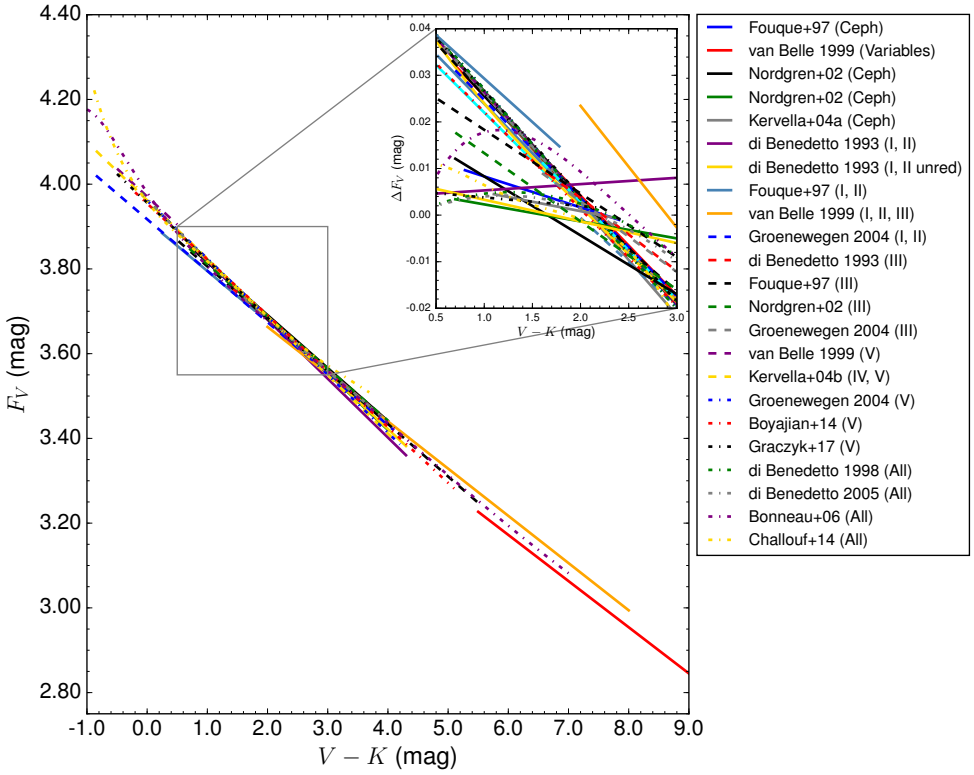

Fig. 1. 23 SBCRs in the literature plotted as a function of the $V-K$ colour (over their validity domain), and comparatively to the Kervella et al. (2004a) relation in ΔF_V on the top right corner, between 0.5 and 3.0 mag, which is taken as a reference (for clarity). We note, however, that the Kervella et al. (2004a) relation is in principle valid only over the −0.85 to 4.10 $V-K$ range. The references for these SCBRs are as follows: Fouque & Gieren (1997), van Belle (1999), Nordgren et al. (2002), Kervella et al. (2004a,b), di Benedetto (1993, 1998, 2005), Groenewegen (2004), Boyajian et al. (2014), Graczyk et al. (2017), Bonneau et al. (2006), and Challouf et al. (2014).

Table 1. Description of the stellar characteristics (top part), interferometric (middle part), and photometric (bottom) criteria we considered for the data selection.

	Criterion	Label
Stellar characteristics (see Sect. 3.3)	Variable [(a)]	V
	Spectroscopic binary	SB
	Multiple	M
	Doubt on luminosity class	LumC
	Semi-regular pulsating star	Sr Puls
	Fast rotator	FRot
Interferometric (see Sect. 3.4)	Not compatible data and no visibility curve	NVisC
	8−13 μm band	8−13
	Data very far from the general trend	Bad
	High visibility measurements ($V^2 > 0.8$)	hVis
	Excellent visibility curve in the other reference [(b)]	eVisC
	Large visible band problem	LvisBand
Photometric (see Sect. 3.6)	High K magnitude uncertainty	hK

Notes. Right column shows labels relative to these criteria, which we included as a note in the final samples of stars (see Table 3). [(a)]BY: BY Dra type, TT: T Tauri type, RS: RS CVn type, dS: δ Scuti type, Cep: Cepheids. [(b)]In case of inconsistent redundancies.

However, we needed to make several exceptions in the selection process. Among the remaining stars, the variability was prevalent in the F5/K7 giants sample. This criterion is thus not considered when selecting giants. We quantitatively study this point later in Sect. 5.1. Moreover, given the very low number of M dwarf measurements, no selection is based on their activity (only the quality of the interferometric data, see below).

3.4. Interferometric criteria

To build accurate SBCRs, one needs precise angular diameter measurements. We arbitrarily excluded measurements with errors on the angular diameter larger than 8%. We then removed measurements done in the 8−13 μm band to avoid the contamination of the flux of the star by any materials, like a circumstellar envelope or dust. In some cases, we find data that is totally inconsistent (more than 5σ) with the SBCRs, due to inaccurate conversions from $\theta_{\rm UD}$ to $\theta_{\rm LD}$, bad observation quality and/or poor spatial frequency coverage in the visibility curve. The corresponding data are then flagged as "NVisC", "Bad" or "LvisBand" in Table 1. If a star has several interferometric independent measurements (e.g. on different instruments) satisfying all the criteria, we keep them all in the sample.

The LD diameters in the JMDC are predominantly deduced from the measured UD diameters using Claret's grids (Claret et al. 1995; Claret 2000; Claret & Bloemen 2011). Claret's grids

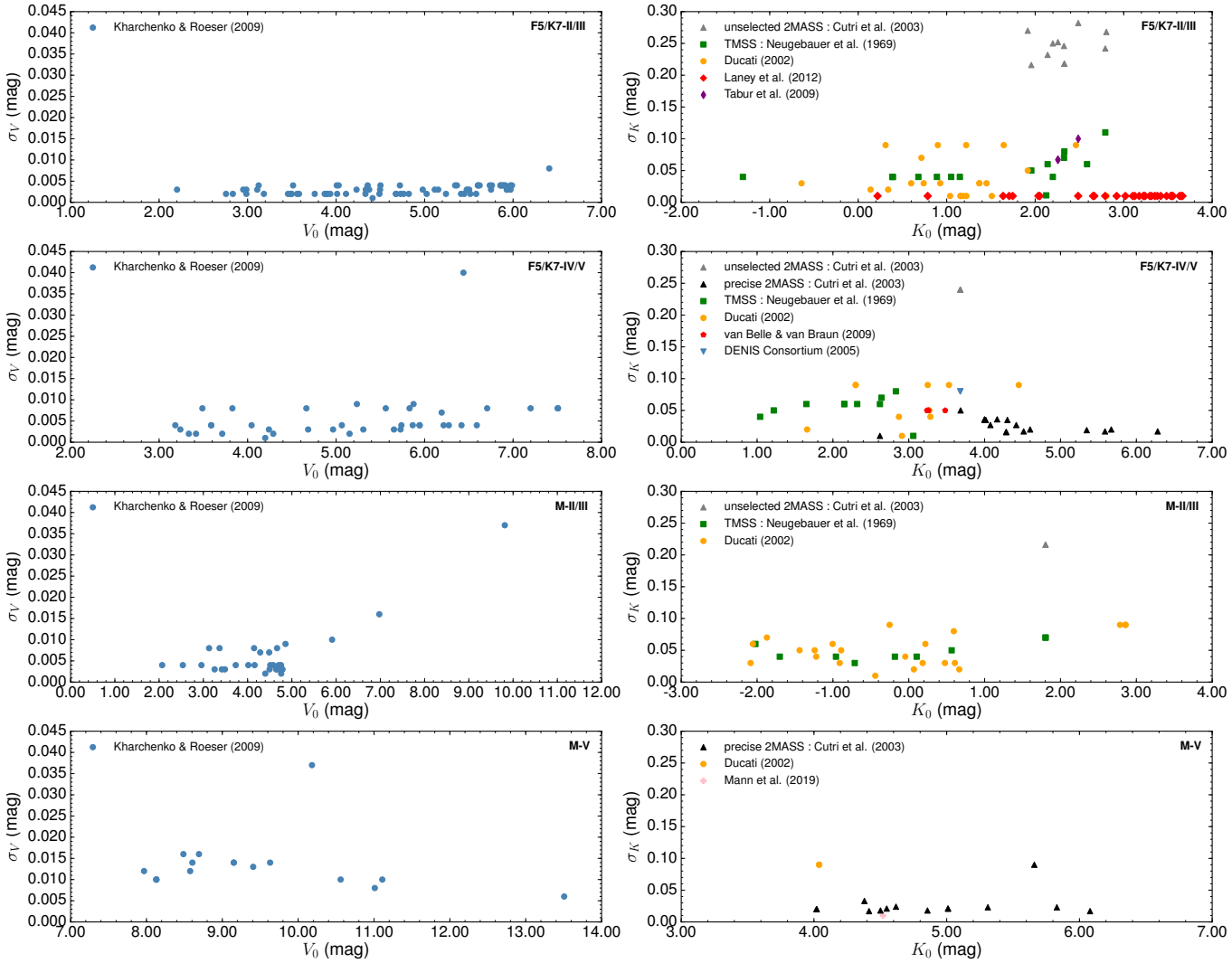

Fig. 2. σ_V vs. V_0 (*left panels*) and σ_K vs. K_0 (*right panels*) plotted for the four samples, indicated in the top-right corner of each graphic. The photometric sources are noted in the legend.

have a step of 250 K in temperature, thus the largest error we can make on the temperature is 125 K without any interpolation. As mentioned by Nardetto et al. (2020) in a recent work, this error on the temperature leads to an error of 0.3% on all angular diameters, well below the typical errors of our samples. Moreover, the angular diameters computed with SATLAS (Lester & Neilson 2008; Neilson & Lester 2013) are 0.4% larger from those deduced with Claret & Bloemen (2011) grids for K giants. For dwarfs, we expect an even smaller difference. This means that even if the UD to LD conversion is not done homogeneously on our JMDC samples, the impact on the value of the angular diameter is well below the quoted uncertainty.

3.5. Visible photometry

Surface brightness–colour relations are strongly dependent on the photometry used for the calibration. We thus took into consideration both V and K uncertainties to properly build our SBCR fitting strategy. We considered visible magnitudes from the Kharchenko & Roeser (2009) catalogue. This catalogue gathers measurements from several other catalogues (HIPPARCOS-*Tycho* catalogues, Carlsberg Meridian Catalog and the Positions and Proper Motions catalogue), and all the visible magnitudes are given in the Johnson V filter. The strong interest of this catalogue is the accuracy of the measurements, with an error on the visible magnitude rarely exceeding 0.01 mag (see Fig. 2).

3.6. Infrared photometry and additional criterion

The uniformity of the infrared K magnitude was more complicated to fulfill since the 2MASS catalogue (Cutri et al. 2003), which is the most complete catalogue of infrared photometry, is not very accurate for a lot of the measurements (mainly because of saturation issues). We decided to consider only infrared measurements with an error below 0.15 mag. For stars with a precision larger than 0.15 mag on the 2MASS photometry, we searched other catalogues for more accurate infrared measurements. This allowed us to keep 10 additional stars, indicated by grey triangles in Fig. 2, for which we found more precise infrared photometry. The various sources we found for the infrared photometry are given in the legend in Fig. 2. They are also listed in Table 2 with their corresponding labels. This induced a new selection criterion, labelled as "hK".

Among all the catalogues we use for the infrared K-photometry, only Ducati (2002) and Neugebauer & Leighton (1969) use Johnson photometry without conversion into 2MASS

Table 2. Infrared photometry sources with their corresponding labels included in Table 1.

Infrared photometry source	Label
TMSS (Neugebauer & Leighton 1969)	T
Ducati (2002)	Du
2MASS (Cutri et al. 2003)	2M
DENIS Consortium (2005)	De
van Belle & von Braun (2009)	V
Tabur et al. (2009)	Ta
Laney et al. (2012)	La
Mann et al. (2019)	M19

photometry. This corresponds to 85 stars over the 153 in our samples. We did a test by considering only Ks photometries to constrain our SBCRs. We find a consistency of less than 1-σ between the one with only 2MASS photometry and the other one with heterogeneous photometry. To evaluate the impact of the heterogeneous infrared photometry, we compared both photometries for 4 stars in our samples: HD 140283, HD 3651, HD 4628, and HD 75732. We found a difference of 0.05%, 0.35%, 2.5%, and 1.2%, respectively, leading to a difference of 0.1%, 0.7%, 4.5%, and 2.8% on the angular diameter. Both K and K_s photometries are consistent in the error bars for these four stars. The difference is therefore minimal, provided that K and K_s photometries differ within 2%. To conclude, our SBCRs are mixed with 2MASS/Johnson $-K$ photometries, but both are consistent, meaning that our SBCRs can be used with the two photometries without including any significant bias on the angular diameter.

3.7. Reddening corrections

We used the *Stilism*[2] online tool (Lallement et al. 2014; Capitanio et al. 2017) to compute the colour excess $E(B-V)$. This tool produces tridimensional maps of the local interstellar matter (ISM) based on measurements of starlight absorption by dust (reddening effects) or gaseous species. By definition, the interstellar attenuation A_V in the visible band is given by

$$A_V = R_V \times E(B-V), \tag{5}$$

where R_V is the ratio of total to selective absorption in the visible band, for which we adopted $R_V = 3.1$, which corresponds to the typical value in the diffuse ISM (Cardelli et al. 1989). We then used $A_K = 0.119 \times A_V$, according to Nishiyama et al. (2009).

It is well known that the SBCR is not significantly sensitive to the reddening correction, since the magnitude absorption is compensated by the colour extinction. The visual absorption of our samples rarely exceeds 0.1 mag. To quantify its contribution, we increased the value of the visual extinction on a few stars of our F5/K7 giants sample. A high value $A_V = 0.1$ mag yields to a difference of 0.3% on the surface brightness, and 0.35% on the resulting angular diameter. Nardetto et al. (2020) did a test by varying the visible absorption A_V on their entire sample. They find that for a larger absorption of 0.1 mag, the zero-point of their SBCR increases by 0.045 mag (i.e. 0.0045 mag in the F_V definition), which roughly corresponds to the rms of their relation.

The contribution of the visual extinction to the SBCR is therefore minimal. However, we decided to take into consideration the extinction since the colour validity interval of the relation can be impacted.

[2] The online tool is available at http://stilism.obspm.fr

4. Determination of new surface brightness–colour relations

4.1. Final selected measurements samples

With the methodology described in Sect. 3, we obtain four samples of carefully selected measurements, depending on luminosity classes. All the tables (including selected and rejected stars) are provided at the CDS. The four tables have the following numbers of selected stars (selected/total[3]): F5/K7–II/III (70/274), F5/K7–IV/V (38/156), M–II/III (29/67), M–V (16/37). As an example, the F5/K7 giants sample is shown in Table 3, including keywords relative to the source of the infrared photometry, as well as specific keywords corresponding to criteria of selection indicated in the "Notes" column. Final selected measurements are those with an empty cell in the Notes column.

4.2. New specific surface brightness–colour relations

The new relations for the four samples are presented in Fig. 3. The SBCRs are listed in Table 4, and we detail our fitting strategy in Appendix A. We did a test by comparing a least-square (LS) regression with our strategy. We find that using a simple LS method leads to a maximum difference of 1% on the angular diameter compared to our method. We therefore decided to keep our fitting strategy, since the difference with the LS method is not significant. We consider our method as more robust as we take into consideration all uncertainties that could induce a bias in the final SBCR.

The most precise relation is found for the F5/K7 giants working box, with an rms of 0.00223 mag. The resulting angular diameter is obtained from Eq. (3) as follows:

$$\theta_{\rm LD} = 10^{8.4392-0.2V_0-2F_{V_0}}. \tag{6}$$

A formal way to calculate the expected angular diameter precision $\sigma_{\theta_{\rm LD}}$ is to apply the partial derivative method on Eq. (6):

$$\frac{\sigma_{\theta_{\rm LD_{rms}}}}{\theta_{\rm LD}} = 2\ln(10)\sigma_{\rm rms}. \tag{7}$$

This leads to a precision of 1% on the estimation of the angular diameter in the case of F5/K7 giants. Regarding the other boxes, the rms of the relations range from 0.00377 mag to 0.00461 mag, leading to an estimate of the angular diameter precision between 1.7% and 2.1%. As shown in Table 4, the $V-K$ colour domain of validity of these relations ranges from 1 to 7.5 mag.

However, one should notice that such precision corresponds to a lower limit on the expected angular diameter uncertainty. Indeed, if we want to deduce the angular diameter using a SBCR, we have to consider the uncertainties on the colour and the coefficients of the SBCR. The total resulting uncertainty on the angular diameter can be expressed as $\theta_{\rm LD} \pm \sigma_{\theta_{\rm LD_{rms}}} \pm \sigma_{\theta_{\rm LD_{a,b,phot}}}$, where $\sigma_{\theta_{\rm LD_{a,b,phot}}}$ is given by

$$\sigma_{\theta_{\rm LD_{a,b,phot}}} = 2\ln(10)\theta_{\rm LD}\sigma_{\theta_{\rm LD_{a,b}}}\sigma_{\theta_{\rm LD_{phot}}}, \tag{8}$$

where

$$\sigma_{\theta_{\rm LD_{a,b}}} = \left\{[(V-K)-0.881A_V]^2\,\sigma_a^2 + \sigma_b^2\right\}^{1/2} \tag{9}$$

[3] The total number of measurements is the number of measurements remaining after applying common criteria to the JMDC.

Table 3. Part of the F5/K7 giants sample after applying common criteria.

Name	θ_{LD} [mas]	$\sigma_{\theta_{LD}}$ [mas]	Band	Source	Sp. type	V [mag]	σ_V [mag]	K [mag]	σ_K [mag]	A_{λ_V} [mag]	K ref.	Notes
HD 100407	2.394	0.029	K	Thévenin et al. (2005)	G7IIIb	3.535	0.002	1.47	0.252	0.0031	2M	M
HD 10142	0.964	0.0060	H	Gallenne et al. (2018)	K0III	5.933	0.003	3.557	0.010	0.0031	La	
HD 102328	1.606	0.0060	K'	Baines et al. (2010)	K2.5IIIbCN1	5.254	0.002	2.488	0.100	0.0124	Ta	
HD 103605	1.098	0.0090	K'	Baines et al. (2010)	K1III	5.827	0.002	3.102	0.298	0.0248	2M	hK
HD 10380	2.81	0.03	740 nm	Nordgren et al. (1999)	K3III	4.435	0.003	1.356	0.307	0.031	2M	NVisC
HD 104985	1.032	0.022	2.15	Baines et al. (2008)	G8.5IIIb	5.785	0.003	3.273	0.303	0.0217	2M	M
HD 106574	1.498	0.027	K'	Baines et al. (2010)	K2III	5.721	0.003	2.94	0.08	0.0403	T	hVis
HD 108381	2.179	0.057	550−850 nm	Baines et al. (2018)	K1IIIFe0.5	4.339	0.003	1.809	0.250	0.0031	2M	Bad + LvisBand
HD 11092	2.797	0.019	H or K	van Belle et al. (2009)	K4Ib-IIa	6.548	0.004	1.784	0.239	1.2679	2M	LumC
HD 113049	0.971	0.021	K'	Baines et al. (2010)	K0III	5.993	0.004	3.658	0.312	0.0403	2M	hK
HD 113226	3.17	0.02	740 nm	Nordgren et al. (1999)	G8III-IIIb	2.836	0.002	0.786	0.010	0.0031	La	eVisC
HD 113226	3.283	0.033	800 nm	Mozurkewich et al. (2003)	G8III-IIIb	2.836	0.002	0.786	0.010	0.0031	La	
HD 113226	3.318	0.013	550−850 nm	Baines et al. (2018)	G8III-IIIb	2.836	0.002	0.786	0.010	0.0031	La	Bad + LvisBand
HD 113996	3.09	0.019	550−850 nm	Baines et al. (2018)	K5-III	4.782	0.002	1.2	0.09	0.0155	Du	Bad + LvisBand
HD 118904	1.871	0.032	K'	Baines et al. (2010)	K2III	5.493	0.003	2.69	0.07	0	T	Bad
HD 11977	1.528	0.013	H	Gallenne et al. (2018)	G5III	4.684	0.002	2.486	0.01	0.0062	2M	
HD 120477	4.691	0.022	550−850 nm	Baines et al. (2018)	K5.5III	4.041	0.004	0.34	0.02	0.0124	Du	Bad + LvisBand
HD 120477	4.72	0.04	740 nm	Nordgren et al. (1999)	K5.5III	4.041	0.004	0.34	0.02	0.0124	Du	
HD 12438	1.091	0.016	H	Gallenne et al. (2018)	G8III	5.348	0.004	3.176	0.010	0.0031	La	
HD 124897	20.95	0.2	2.2	di Benedetto & Foy (1986)	K1.5IIIFe-0.5	0.085	0.009	−2.911	0.170	0	2M	M
HD 124897	21.373	0.247	800 nm	Mozurkewich et al. (2003)	K1.5IIIFe-0.5	0.085	0.009	−2.911	0.170	0	2M	M
HD 124897	21.6	1.2	2.2	di Benedetto & Conti (1983)	K1.5IIIFe-0.5	0.085	0.009	−2.911	0.170	0	2M	M
HD 127665	3.901	0.0080	550−850 nm	Baines et al. (2018)	K3-III	3.571	0.002	0.6	0.03	0.0124	Du	
HD 12929	6.792	0.043	700 nm	Hutter et al. (2016)	K2-IIIbCa-1	2.01	0.004	−0.782	0.175	0	2M	M
HD 12929	6.827	0.068	800 nm	Mozurkewich et al. (2003)	K2-IIIbCa-1	2.01	0.004	−0.782	0.175	0	2M	M
HD 12929	6.85	0.9	800 nm	Mozurkewich et al. (1991)	K2-IIIbCa-1	2.01	0.004	−0.782	0.175	0	2M	M
HD 12929	6.88	0.03	740 nm	Nordgren et al. (1999)	K2-IIIbCa-1	2.01	0.004	−0.782	0.175	0	2M	M
HD 12929	7.6	0.9	550 nm	Faucherre et al. (1983)	K2-IIIbCa-1	2.01	0.004	−0.782	0.175	0	2M	M
HD 12929	8.7	0.5	674 nm	Hutter et al. (1989)	K2-IIIbCa-1	2.01	0.004	−0.782	0.175	0	2M	M
HD 131873	10.301	0.103	800 nm	Mozurkewich et al. (2003)	K4-III	2.063	0.003	−1.286	0.203	0.0031	2M	M
HD 131873	8.9	1.0	550 nm	Faucherre et al. (1983)	K4-III	2.063	0.003	−1.286	0.203	0.0031	2M	M
HD 133124	3.055	0.077	550−850 nm	Baines et al. (2018)	K4III	4.79	0.002	1.23	0.010	0.062	Du	
HD 133208	2.477	0.065	800 nm	Mozurkewich et al. (2003)	G8IIIaFe-0.5	3.476	0.002	1.223	0.165	0.0248	2M	M
HD 133208	2.484	0.0080	550−850 nm	Baines et al. (2018)	G8IIIaFe-0.5	3.476	0.002	1.223	0.165	0.0248	2M	Bad + LvisBand
HD 13468	0.886	0.01	H	Gallenne et al. (2018)	K0III	5.932	0.004	3.666	0.010	0.0186	La	
HD 135722	2.74	0.02	740 nm	Nordgren et al. (1999)	G8IIIFe-1	3.466	0.002	1.19	0.01	0.0093	Du	eVisC
HD 135722	2.764	0.03	800 nm	Mozurkewich et al. (2003)	G8IIIFe-1	3.466	0.002	1.19	0.01	0.0093	Du	
HD 1367	0.754	0.013	H	Ligi et al. (2016)	K0III	6.177	0.004	4.224	0.263	0.0155	2M	hK
HD 136726	2.149	0.023	550−850 nm	Baines et al. (2018)	K4III	5.013	0.003	1.92	0.05	0.0341	T	
HD 136726	2.336	0.020	K'	Baines et al. (2010)	K4III	5.013	0.003	1.92	0.05	0.0341	T	eVisC
HD 13686	1.581	0.063	H or K	van Belle et al. (2009)	K2.5Ib-II	7.03	0.004	2.709	0.335	1.891	2M	LumC
...	...	...	...	...	...	...	...	...	...	...	...	...

Notes. The "Notes" column contains keywords relative to stellar characteristics, interferometric and photometric criteria when the star is not considered. Refer to Table 1 for a description of these keywords. "K ref" column includes infrared photometry sources as listed in Table 2.

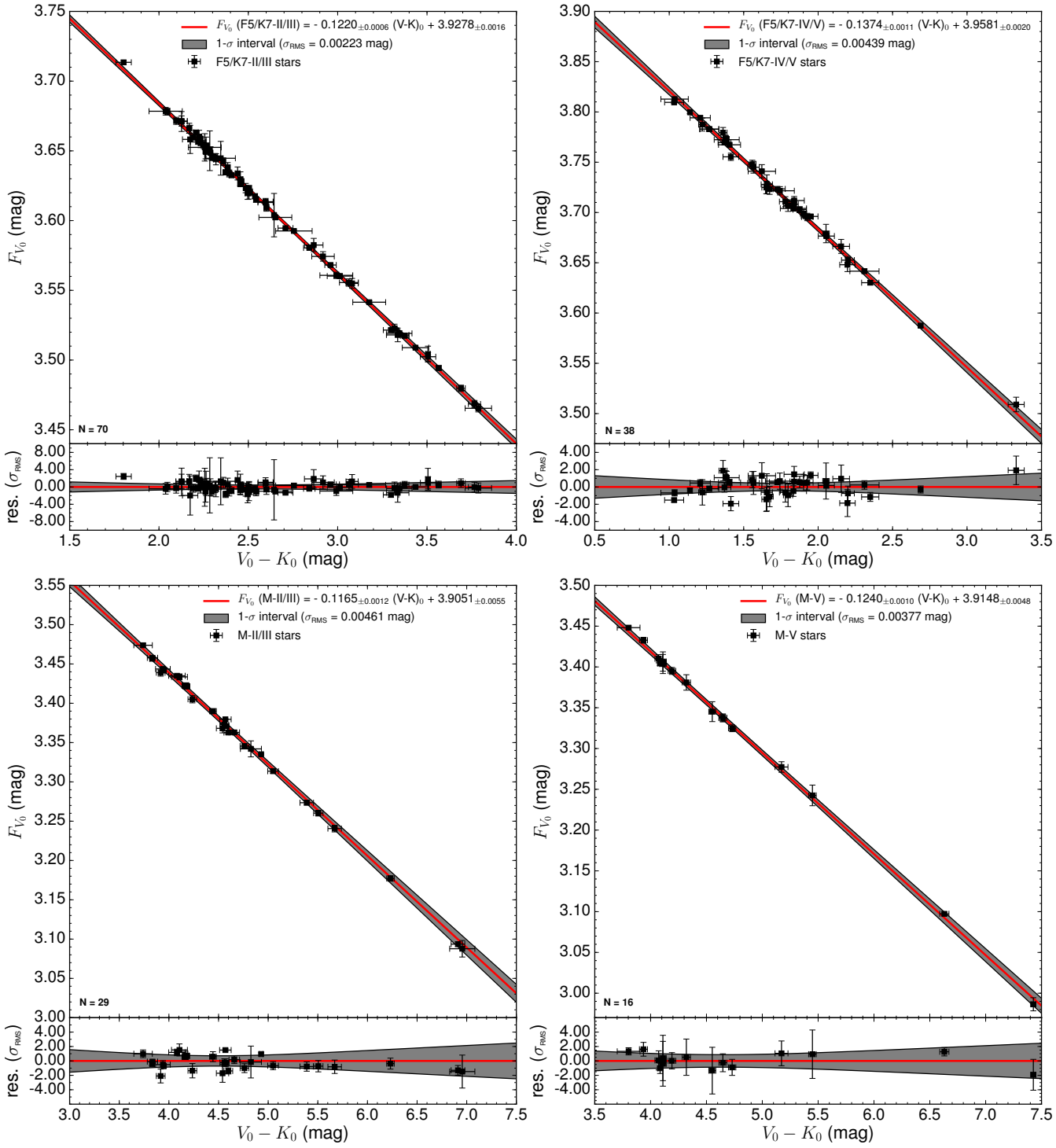

Fig. 3. Newly developed surface brightness–colour relations after applying stellar characteristics, interferometric and photometric criteria. *From top-left to bottom-right panel*: SBCRs for F5/K7 giants, F5/K7 sub-giants/dwarfs, M giants and M dwarfs. The shaded grey area corresponds to the 1-σ confidence interval computed according to Eq. (A.5). The uncertainty on the surface brightness of each measurement was divided by the rms.

is the uncertainty linked to the coefficients a and b of the relation, and

$$\sigma_{\theta_{\mathrm{LD_{phot}}}} = \left\{a^2 \left(\sigma_V^2 + \sigma_K^2 + 0.014\sigma_{A_V}^2\right)\right\}^{1/2} \quad (10)$$

is the photometric part of the uncertainty. For the F5/K7 giants' relation, by considering only uncertainties due to the coefficients of the SBCR, and fixing an arbitrary colour of $V-K = 3$ mag, we find a precision of 1.10% on the angular diameter. On the other hand, if we consider only arbitrary uncertainties of 0.022 mag on both V and K magnitudes, we get 1.70% precision. If we set σ_V 10% smaller, we are now only sensitive to σ_K and we get 1.20% precision. This means that precise V and K band photometries (<0.022 mag) are necessary if we want to reach 1% precision on the angular diameter using an SBCR with a rms of 0.00223 mag.

A number of interferometric measurements have uncertainties below 1%. We did a test by setting a lower limit of 1% on the angular diameter and 0.03 mag on the $V-K$ colour of the stars.

Table 4. Parameters of the new SBCRs.

Working box	Number of data	Relation	$(V-K)$ range [mag]	$\sigma_{\rm rms}$ [mag]	Expected $\frac{\sigma_{\theta_{\rm LD}}}{\theta_{\rm LD}}$ [%]
F5/K7–II/III	70	$F_{V_0} = -0.1220_{\pm 0.0006}(V-K)_0 + 3.9278_{\pm 0.0016}$	[1.80; 3.80]	0.00223	1.03
F5/K7–IV/V	38	$F_{V_0} = -0.1374_{\pm 0.0011}(V-K)_0 + 3.9581_{\pm 0.0020}$	[1.00; 3.30]	0.00439	2.02
M–II/III	29	$F_{V_0} = -0.1165_{\pm 0.0012}(V-K)_0 + 3.9051_{\pm 0.0055}$	[3.70; 7.00]	0.00461	2.12
M–V	16	$F_{V_0} = -0.1240_{\pm 0.0010}(V-K)_0 + 3.9148_{\pm 0.0048}$	[3.80; 7.50]	0.00377	1.73

Notes. The $(V-K)$ range column denotes the validity interval of the relation.

The SBCRs we obtained were consistent at less than 1-σ with the current ones. A possible under-estimation of the uncertainties therefore has no impact on our SBCRs.

5. Discussion

5.1. Different surface brightness–colour relations for giants and dwarfs, and a comparison with the literature

In Fig. 4, we superimposed our SBCRs with various relations found in the literature, namely Kervella et al. (2004a), Boyajian et al. (2014), Pietrzyński et al. (2019), and Adams et al. (2018). In Fig. 5, we compare our own relations for giant and dwarf stars, respectively. This shows that using the F5/K7 relation for giants, instead of the one for dwarfs, leads to an error on the estimation of the angular diameter of up to 9%. The disagreement can even reach 18% for the M relations. Using relations adapted to the spectral type and class of the star is therefore mandatory. This result is consistent with several previous studies (di Benedetto 1993; Fouque & Gieren 1997; Groenewegen 2004; Kervella et al. 2004a).

As mentioned in Sect. 3.3, we decided to ignore the variability criterion for F5/K7 giants. After a case-by-case analysis, we found in Kukarkin et al. (1981) that the variability generates a noise on the V magnitude between ±0.02 and ±0.10 mag, with a median value at 0.04 mag. Removing variables from the sample leads to a relation in very good agreement at a level of 0.2σ with the current one, but keeping variables does not influence the calibration of our SBCRs.

Recently, Adams et al. (2018) considered 78 giants, sub-giants, and dwarfs, with interferometric angular diameter estimates at the 2% level or better (and observed on at least two separated occasions), in order to constrain the SBCRs. They used different coulours and a definition of the SBCR compared to the one we use in this work (including V and K), and they paid attention to binarity, following the selection strategy described in Boyajian et al. (2008). They reached the conclusion (conversely to other authors mentioned above) that there is no difference between the SBCRs of giants, sub-giants, and dwarfs, and they obtained a precision of 3% in the $V-K$ colour system. Figures 6 and 7 show the normalised difference (in %) on the angular diameter we expect between our SBCRs and relations taken from the literature, introduced above. For dwarfs and sub-giants, we obtained different results to Adams et al. (2018) on the derived angular diameters of at most 6% over their domain of validity. For F5/K7 and M giants, we respectively obtained a good agreement at the 1.5% and 2.5% levels.

Chelli et al. (2016) developed a new method for the calibration of the SBCR based on the differential surface brightness (DSB) and pseudo-magnitudes. Similarly to Adams et al. (2018), they found a unique polynomial solution for all stars (dwarfs and giants), as a function of the spectral type. This relation gives a precision of about 3% on the derived angular diameters. If we apply the same methodology of DSB and pseudo-magnitudes on our samples, we obtain a comparable precision to the one obtained for our SBCRs, and, importantly, we again retrieve different DSB relations between giants and dwarfs.

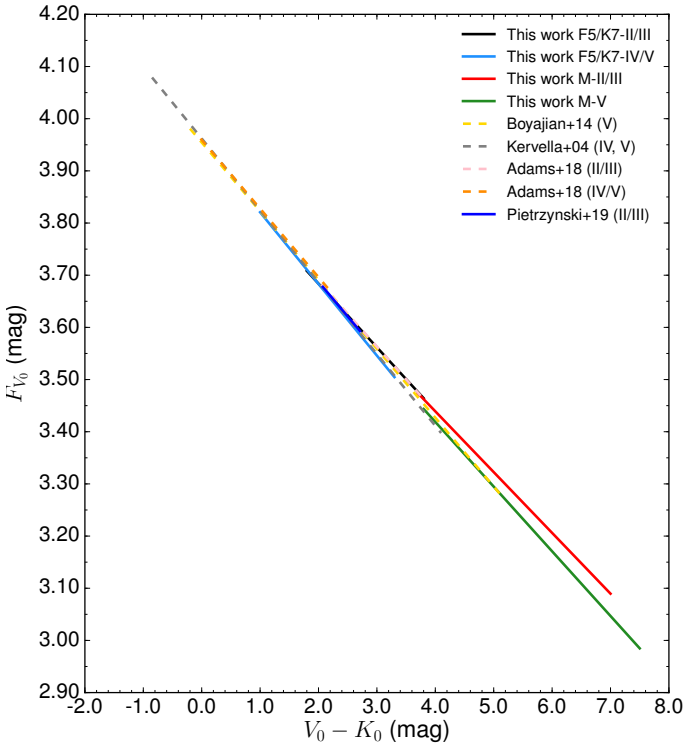

Fig. 4. Comparison between our four newly developed SBCRs with relations in the literature.

The precision we reached with the F5/K7 giants' SBCR is comparable to the one of Pietrzyński et al. (2019). As shown in Fig. 6, we expect a difference of at most 2% on the angular diameter with the SBCR of Pietrzyński et al. (2019). This difference could be due to the fact that we considered observational and stellar characteristics selection criteria. We indeed rejected 21 stars among 48 observed by Pietrzyński et al. (2019) because of their activity, despite the very good quality of the observations. The agreement between the relations is lower than 1.5% for the majority of the colour range considered. On the other hand, we find very good agreement between our F5/K7–IV/V SBCR and that of Kervella et al. (2004a). Using one or the other relation leads to a difference of less than 1% on the angular diameter, which reveals a strong consistency of these two SBCRs. However, our M–V relation is inconsistent with the SBCR of Kervella et al. (2004a) at a level of more than 4%, but consistent

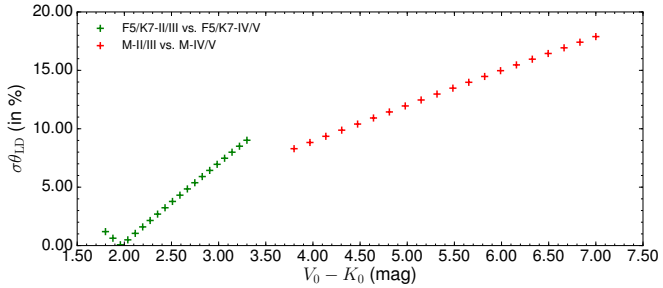

Fig. 5. Difference (in %) of angular diameter estimations between our SBCRs.

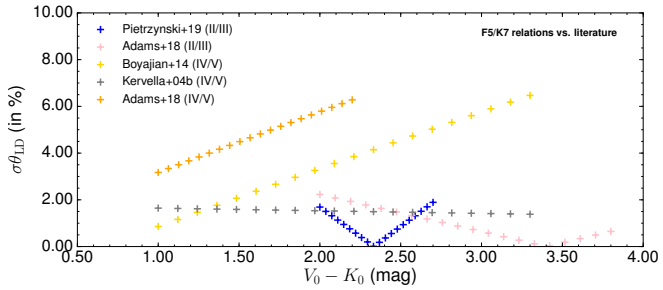

Fig. 6. Difference (in %) of angular diameter estimations between our F5/K7 relations and the literature.

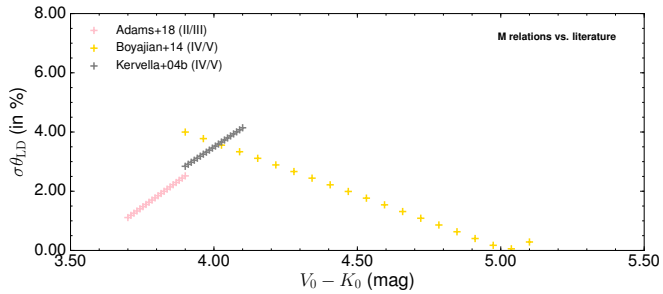

Fig. 7. Difference (in %) of angular diameter estimations between our M relations and the literature.

with Boyajian et al. (2014) under 2.5%. We need new data and complementary works to understand these differences.

5.2. Surface brightness–colour relations for Gaia

In this section, we convert our SBCRs in the *Gaia* photometric band G. The G photometry of the stars in our sample is found in the *Gaia* DR2 database (Gaia Collaboration 2018). In order to determine the corresponding extinction (A_G), we used an analytic model established by Danielski et al. (2018):

$$A_G = a_1 + a_2(G-K)_0 + a_3(G-K)_0^2 + a_4(G-K)_0^3 + a_5 A_V + a_6 A_V^2 + a_7(G-K)_0 A_V, \quad (11)$$

with $a_1 = 0.935556283$, $a_2 = -0.090722012$, $a_3 = 0.014422056$, $a_4 = -0.002659072$, $a_5 = -0.030029634$, $a_6 = 0.000607315$, and $a_7 = 0.002713748$. The SBCRs based on the *Gaia* photometry are shown in Fig. 8, while their coefficients are listed in Table 5. We find a good consistency with the SBCR based on the V band. Precision ranges from 1.1% to 2.4%.

There are several things to mention. First, we did not find the G photometry for six of the giant stars. Second, one M–II/III star is totally incompatible with the SBCR, namely HD 236459 (red point on the bottom-left panel of Fig. 8). Taking a look at this star, its distance is found to be about 2.3 kpc (i.e. much further than the distance of the other giants in our sample), leading to a very high visible extinction of $A_V = 1.80$ mag. This star has been removed for the fit of the SBCR.

5.3. Validating our methodology with recent interferometric measurements

To go further in the validation of our methodology, we selected 10 new stars for interferometric observations with both the Precision Astronomical Visible Observations (PAVO) (Ireland et al. 2008) and the Visible spEctroGraph and polArimeter (VEGA) (Mourard et al. 2009, 2011) instruments. These instruments are installed on the Center for High Angular Resolution Astronomy (CHARA) array, in Mount Wilson, USA (ten Brummelaar et al. 2005). Comparing interferometric measurements from different instruments serves to support the importance of such selection criteria to implement our SBCRs. The ten stars were observed between July 2013 and August 2016 with PAVO, and from August 2012 to June 2019 with VEGA. They have spectral types between G6 and K3. Eight of them are giants, one is a sub-giant and one is a dwarf. The data analysis and results of VEGA measurements are briefly presented here, while the PAVO measurements, as well as a careful comparison of the VEGA and PAVO data will be presented in a forthcoming separate paper (Creevey et al., in prep.). For the data analysis, we used the standard approach described in Mourard et al. (2009, 2011). We fitted a limb-darkening model to the VEGA visibility measurements using the LITpro software (Tallon-Bosc et al. 2008). The u_R linear to limb-darkening coefficient for each star was found using the Claret & Bloemen (2011) catalogue. Results are shown on the top part of Table 6. The corresponding visibility curves are included in Fig. B.1 of the appendix. In order to complete the analysis, we also added four giant stars, recently observed by CHARA/VEGA and presented in Nardetto et al. (2020). They compare their limb-darkened angular diameters to the ones derived in the H-band with the Precision Integrated Optics Near-infrared Imaging ExpeRiment (PIONIER) (Le Bouquin et al. 2011) on VLTI. Results are listed in the bottom part of Table 6. The important point is that all stars in Table 6 have been observed by two different instruments, and the derived angular diameters are found to be consistent at the 1σ level. These limb-darkened angular diameters are thus extremely robust.

Left and right panels of Fig. 9 show the ten stars observed by VEGA and PAVO on their corresponding SBCR. We find that these stars are not consistent with our relations at a level of up to 12σ. Looking at the selection criteria described in Sect. 3, these stars should be rejected from the sample, because of multiplicity, variability, and poor K photometry, as indicated in the Notes column of Table 6. This result demonstrates the importance of the selection criteria that we have defined. The four giant stars observed by VEGA and PIONIER (Nardetto et al. 2020) fulfill all the selection criteria. The results are shown in Fig. 10 above the F5/K7 giants' relation. As expected, the measurements are totally consistent with the SBCR at a level of ∼1.5%. This supports the existence of such selection criteria to constrain SBCRs.

6. Conclusion and perspectives

We considered all the interferometric measurements of angular diameters obtained so far in order to build accurate SBCRs. We

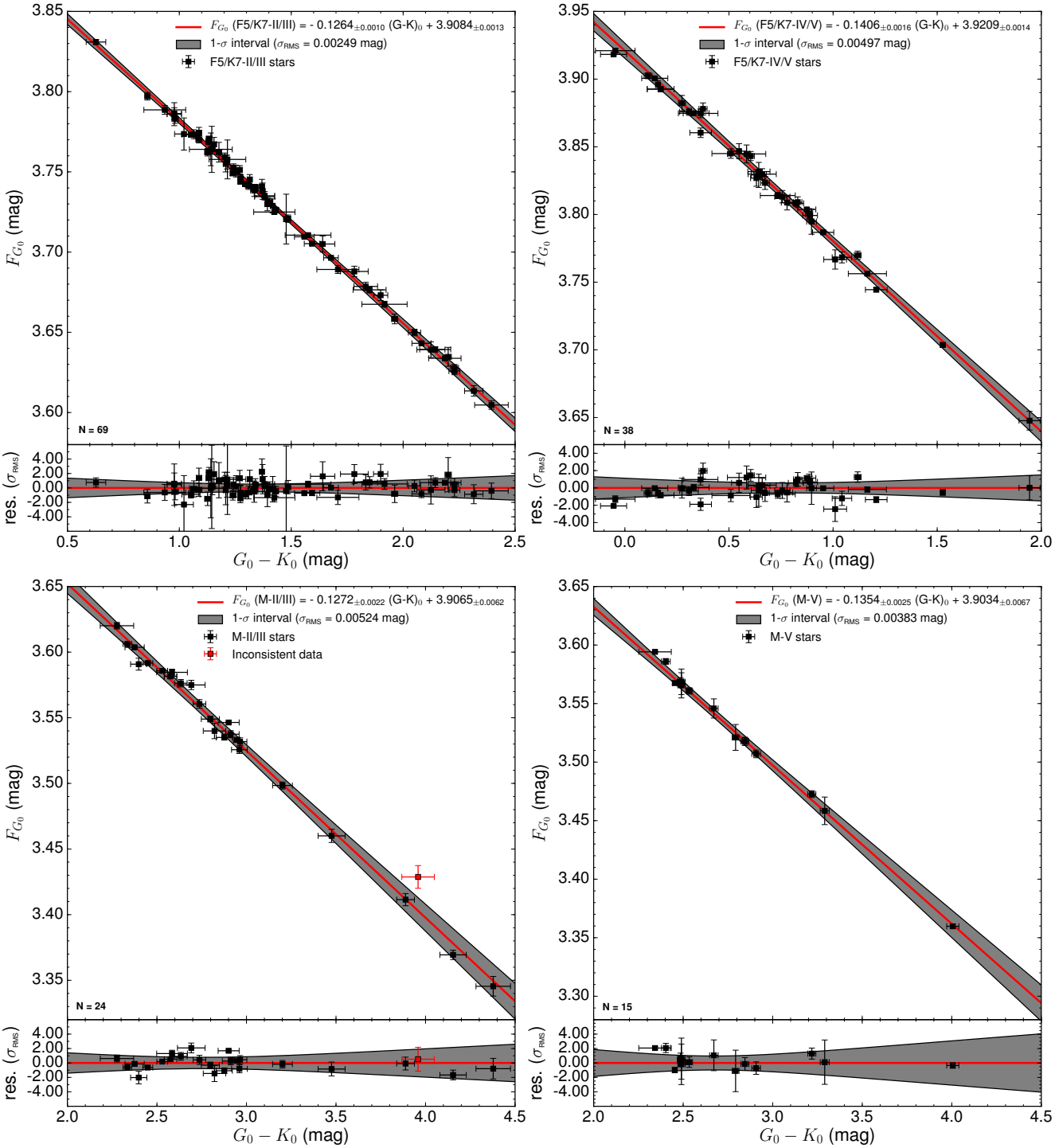

Fig. 8. Surface brightness–colour relations based on the (G, $G-K$) photometric system. *From top-left to bottom-right panel*: SBCRs for F5/K7 giants, F5/K7 sub-giants/dwarfs, M giants, and M dwarfs. The shaded grey area corresponds to the 1-σ confidence interval computed according to Eq. (A.5).

also refined the methodology by homogeneously applying a list of selection criteria. Combining our new VEGA interferometric measurements with those of Nardetto et al. (2020) and Creevey et al. (in prep.), we demonstrated the coherence of our criteria and the importance they have in the determination of the SBCRs. The variability, the multiplicity, along with other stellar characteristics diagnostics, or even the quality of the interferometric observations, as well as the spatial frequency coverage, appear to be of high importance in building consistent SBCRs.

Using this approach, we reinforce the conclusion that the surface brightness of a star depends on its spectral type and its luminosity class, since our new SBCRs for giants and sub-giants/dwarfs are inconsistent with each other at a level of up to 18% on the derived angular diameter, depending on the SBCR considered. Using these criteria, we developed four SBCRs that allow us to estimate angular diameters with an accuracy between 1% and 2%, as soon as the precision of the magnitude of the star is better than 0.04 mag.

Table 5. Parameters of the new SBCRs considering *Gaia* photometry.

Working box	Number of data	Relation	$(G-K)$ range [mag]	$\sigma_{\rm rms}$ [mag]	Expected $\frac{\sigma_{\theta_{\rm LD}}}{\theta_{\rm LD}}$ [%]
F5/K7–II/III	69	$F_{G_0} = -0.1264_{\pm 0.0010}(G-K)_0 + 3.9084_{\pm 0.0013}$	[0.50; 2.40]	0.00249	1.15
F5/K7–IV/V	38	$F_{G_0} = -0.1406_{\pm 0.0016}(G-K)_0 + 3.9209_{\pm 0.0014}$	[−0.10; 2.00]	0.00497	2.29
M–II/III	24	$F_{G_0} = -0.1272_{\pm 0.0022}(G-K)_0 + 3.9065_{\pm 0.0062}$	[2.20; 4.40]	0.00524	2.41
M–V	15	$F_{G_0} = -0.1354_{\pm 0.0025}(G-K)_0 + 3.9034_{\pm 0.0067}$	[2.30; 4.00]	0.00383	1.77

Notes. The $(G-K)$ range column denotes the validity interval of the relation.

Table 6. Our new VEGA angular diameter measurements for ten stars (top) and VEGA measurements from Nardetto et al. (2020) (bottom).

Name	Sp. type	A_V [mag]	$(V-K)_0$ [mag]	u_R	$\theta_{\rm LD}$ [mas]	χ^2_r	Notes
HD 167042	K1III	0	$2.415_{\pm 0.242}$	0.649	$0.831_{\pm 0.068}$	2.994	hK
HD 175740	G8III	0	$2.484_{\pm 0.063}$	0.651	$1.145_{\pm 0.012}$	0.635	M
HD 178208	K3III	0.053	$2.869_{\pm 0.282}$	0.723	$1.071_{\pm 0.011}$	0.480	SB
HD 180756	G8III	0.037	$2.025_{\pm 0.040}$	0.635	$0.683_{\pm 0.016}$	0.214	V
HD 181069	K1III	0.062	$2.478_{\pm 0.040}$	0.692	$0.763_{\pm 0.010}$	0.511	V
HD 181597	K1III	0	$2.660_{\pm 0.292}$	0.695	$0.892_{\pm 0.007}$	0.274	hK
HD 182896	K0III	0.053	$2.643_{\pm 0.026}$	0.707	$0.710_{\pm 0.024}$	0.375	V
HD 185657	G6V	0	$2.370_{\pm 0.220}$	0.641	$0.726_{\pm 0.006}$	0.401	SB
HD 21467	K0IV	0	$2.433_{\pm 0.222}$	0.664	$0.881_{\pm 0.011}$	0.473	M
HD 73665	G8III	0	$2.138_{\pm 0.018}$	0.660	$0.621_{\pm 0.009}$	0.125	M
HD 13468	G9III	0.028	$2.248_{\pm 0.020}$	0.648	$0.902_{\pm 0.017}$	1.600	–
HD 23526	G9III	0.053	$2.228_{\pm 0.020}$	0.652	$0.920_{\pm 0.028}$	0.600	–
HD 360	G8III	0.028	$2.311_{\pm 0.020}$	0.680	$0.888_{\pm 0.010}$	0.500	–
HD 40020	K2III	0.040	$2.434_{\pm 0.020}$	0.690	$1.033_{\pm 0.022}$	0.400	–

Notes. We included a "Notes" column that refers to selection criteria if the star is concerned.

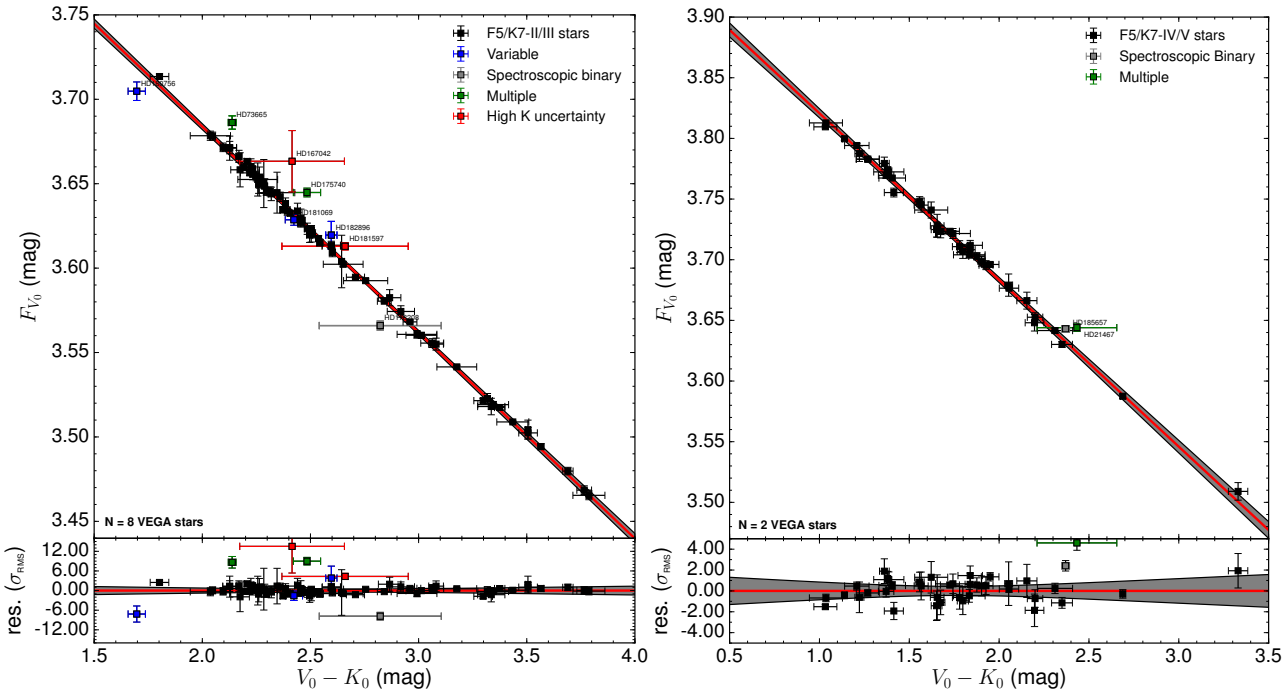

Fig. 9. *Left*: relation for F5/K7 giant stars including the eight new VEGA measurements. *Right*: same for F5/K7 sub-giants/dwarfs with two new VEGA measurements.

The objective is to use these SBCRs in the context of PLATO, in order to infer the radii of stars and planets. Our SBCRs were implemented consistently with the PLATO specifications in terms of spectral type and classes. Moreover, our results are consistent in terms of precision with the PLATO objectives since the spatial mission is expected to bring stellar

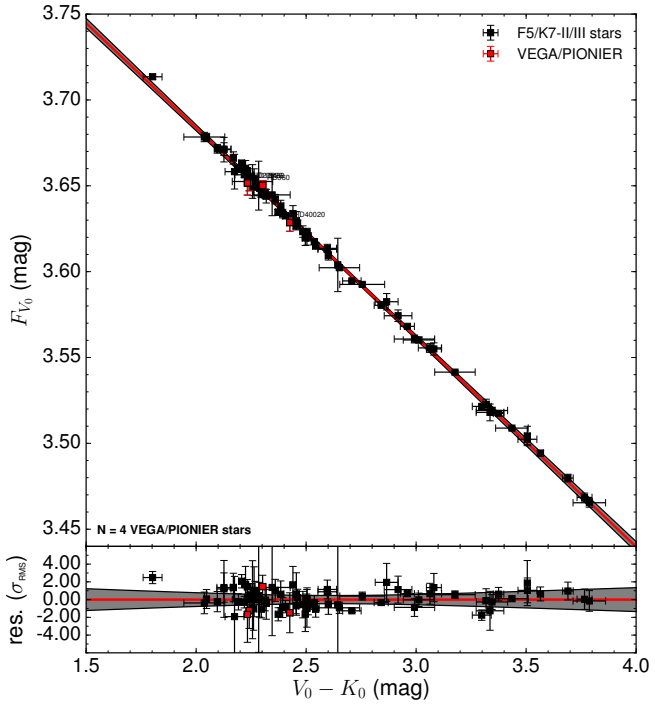

Fig. 10. Relation for F5/K7 giant stars including the four VEGA measurements from Nardetto et al. (2020).

radii measurements with less than 2% precision. However, our sample of stars still has to be enlarged by an order to magnitude in order to improve the robustness of the SBCRs. Using the Stellar Parameters and Images with a Cophased Array (SPICA) instrument at the focus of the CHARA array, we expect to derive the angular diameter of 800 stars in a few years with a 1% precision level (Mourard et al. 2018), which should definitively improve our knowledge of SBCRs. In this context, using the *Gaia* and 2MASS photometric systems, which both have the largest databases, seems to be the best approach.

Since the *Gaia* photometry is among the most homogeneous over the full sky, we calibrate SBCRs using this precise photometry for the first time. We reach a precision on the angular diameter between 1.1% and 2.4%.

Acknowledgements. A.S. acknowledges F. Arenou and N. Leclerc for their contribution to the computation of the interstellar extinction with *Stilism*. This work is based upon observations obtained with the Georgia State University Center for High Angular Resolution Astronomy Array at Mount Wilson Observatory. The CHARA Array is funded by the National Science Foundation through NSF grants AST-0606958 and AST-0908253 and by Georgia State University through the College of Arts and Sciences, as well as the W.M. Keck Foundation. This work made use of the JMMC Measured stellar Diameters Catalog (Duvert 2016). This research made use of the SIMBAD and VIZIER (available at `http://cdsweb.u-strasbg.fr/`) databases at CDS, Strasbourg (France) and the electronic bibliography maintained by the NASA/ADS system. This work has made use of data from the European Space Agency (ESA) mission *Gaia* (`https://www.cosmos.esa.int/gaia`). This research also made use of Astropy, a community-developed core Python package for Astronomy (Astropy Collaboration 2018).

References

Adams, A. D., Boyajian, T. S., & von Braun, K. 2018, MNRAS, 473, 3608
Astropy Collaboration (Price-Whelan, A. M., et al.) 2018, AJ, 156, 123
Baines, E. K., McAlister, H. A., ten Brummelaar, T. A., et al. 2008, ApJ, 680, 728
Baines, E. K., Döllinger, M. P., Cusano, F., et al. 2010, ApJ, 710, 1365
Baines, E. K., Armstrong, J. T., Schmitt, H. R., et al. 2018, AJ, 155, 30
Barnes, T. G., & Evans, D. S. 1976, MNRAS, 174, 489
Bonneau, D., Clausse, J. M., Delfosse, X., et al. 2006, A&A, 456, 789
Boyajian, T. S., McAlister, H. A., Baines, E. K., et al. 2008, ApJ, 683, 424
Boyajian, T. S., van Belle, G. T., & von Braun, K. 2014, AJ, 147, 47
Capitanio, L., Lallement, R., Vergely, J. L., Elyajouri, M., & Monreal-Ibero, A. 2017, A&A, 606, A65
Cardelli, J. A., Clayton, G. C., & Mathis, J. S. 1989, ApJ, 345, 245
Catala, C., & PLATO Team 2006, ESA SP, 1306, 497
Challouf, M., Nardetto, N., Mourard, D., et al. 2014, A&A, 570, A104
Chelli, A., Duvert, G., & Bourgés, L. 2016, A&A, 589, A112
Claret, A. 2000, A&A, 363, 1081
Claret, A., & Bloemen, S. 2011, A&A, 529, A75
Claret, A., Diaz-Cordoves, J., & Gimenez, A. 1995, A&AS, 114, 247
Cutri, R. M., Skrutskie, M. F., van Dyk, S., et al. 2003, VizieR Online Data Catalog: II/246
Danielski, C., Babusiaux, C., Ruiz-Dern, L., Sartoretti, P., & Arenou, F. 2018, A&A, 614, A19
DENIS Consortium 2005, VizieR Online Data Catalog: II/263
di Benedetto, G. P. 1993, A&A, 270, 315
di Benedetto, G. P. 1998, A&A, 339, 858
di Benedetto, G. P. 2005, A&A, 357, 174
di Benedetto, G. P., & Conti, G. 1983, ApJ, 268, 309
di Benedetto, G. P., & Foy, R. 1986, A&A, 166, 204
Ducati, J. R. 2002, VizieR Online Data Catalog: II/237
Duvert, G. 2016, VizieR Online Data Catalog: II/345
Faucherre, M., Bonneau, D., Koechlin, L., & Vakili, F. 1983, A&A, 120, 263
Fouque, P., & Gieren, W. P. 1997, A&A, 320, A799
Gaia Collaboration (Helmi, A., et al.) 2018, VizieR Online Data Catalog: J/A+A/616/A12
Gallenne, A., Kervella, P., Mérand, A., et al. 2017, A&A, 608, A18
Gallenne, A., Pietrzyński, G., Graczyk, D., et al. 2018, A&A, 616, A68
Graczyk, D., Konorski, P., Pietrzyński, G., et al. 2017, ApJ, 837, A7
Groenewegen, M. A. T. 2004, MNRAS, 353, 903
Hutter, D. J., Johnston, K. J., Mozurkewich, D., et al. 1989, ApJ, 340, 1103
Hutter, D. J., Zavala, R. T., Tycner, C., et al. 2016, ApJS, 227, 4
Ireland, M. J., Mérand, A., ten Brummelaar, T. A., et al. 2008, Proc. SPIE, 7013, 701324
Kervella, P., Thévenin, F., Di Folco, E., & Ségransan, D. 2004a, A&A, 426, 297
Kervella, P., Bersier, D., Mourard, D., et al. 2004b, A&A, 428, 587
Kharchenko, N. V., & Roeser, S. 2009, VizieR Online Data Catalog: I/280
Kukarkin, B. V., Kholopov, P. N., Artiukhina, N. M., et al. 1981, Nachrichtenblatt der Vereinigung der Sternfreunde
Lallement, R., Vergely, J. L., Valette, B., et al. 2014, A&A, 561, A91
Laney, C. D., Joner, M. D., & Pietrzyński, G. 2012, MNRAS, 419, 1637
Le Bouquin, J. B., Berger, J. P., Lazareff, B., et al. 2011, A&A, 535, A67
Lester, J. B., & Neilson, H. R. 2008, A&A, 491, 633
Ligi, R., Creevey, O., Mourard, D., et al. 2016, A&A, 586, A94
Mamajek, E. E., Torres, G., Prsa, A., et al. 2015, ArXiv e-prints [arXiv:1510.06262]
Mann, A. W., Dupuy, T., Kraus, A. L., et al. 2019, ApJ, 871, 63
Mourard, D., Clausse, J. M., Marcotto, A., et al. 2009, A&A, 508, 1073
Mourard, D., Bério, P., Perraut, K., et al. 2011, A&A, 531, A110
Mourard, D., Nardetto, N., ten Brummelaar, T., et al. 2018, Proc. SPIE, 10701, 1070120
Mozurkewich, D., Johnston, K. J., Simon, R. S., et al. 1991, AJ, 101, 2207
Mozurkewich, D., Armstrong, J. T., Hindsley, R. B., et al. 2003, AJ, 126, 2502
Nardetto, N. 2018, Habilitation Thesis
Nardetto, N., Salsi, A., Mourard, D., et al. 2020, A&A, 639, A67
Neilson, H. R., & Lester, J. B. 2013, A&A, 554, A98
Neugebauer, G., & Leighton, R. B. 1969, Two-micron Sky Survey. A Preliminary Catalogue (Washington: NASA)
Nishiyama, S., Tamura, M., Hatano, H., et al. 2009, ApJ, 696, 1407
Nordgren, T. E., Germain, M. E., Benson, J. A., et al. 1999, AJ, 118, 3032
Nordgren, T. E., Lane, B. F., Hindsley, R. B., & Kervella, P. 2002, AJ, 123, 3380
Pecaut, M. J., & Mamajek, E. E. 2013, ApJS, 208, 9
Pietrzyński, G., & Gieren, W. 2002, AJ, 124, 2633
Pietrzyński, G., Graczyk, D., Gallenne, A., et al. 2019, Nature, 567, 200
Prša, A., Harmanec, P., Torres, G., et al. 2016, AJ, 152, 41
Tabur, V., Kiss, L. L., & Bedding, T. R. 2009, ApJ, 703, L72
Tallon-Bosc, I., Tallon, M., Thiébaut, E., et al. 2008, Proc. SPIE, 7013, 70131J
ten Brummelaar, T. A., McAlister, H. A., Ridgway, S. T., et al. 2005, ApJ, 628, 453
Thévenin, F., Kervella, P., Pichon, B., et al. 2005, A&A, 436, 253
van Belle, G. T. 1999, PASP, 111, 1515
van Belle, G. T., & von Braun, K. 2009, ApJ, 694, 1085
van Belle, G. T., Creech-Eakman, M. J., & Hart, A. 2009, MNRAS, 394, 1925
Wesselink, A. J. 1969, MNRAS, 144, 297

Appendix A: Fitting strategy

In the traditional case, we suppose that only y is subject to measurement error, and x is observed without error. In this work, we built our fitting strategy around the orthogonal distance regression (ODR), which, contrary to the ordinary least-squares (OLS) regression, considers both x and y errors, respectively errors on the $V-K$ colour and on the surface brightness F_V in our case. If we consider that all variables x_i and y_i are respectively affected by the errors $\delta_i \in \mathbb{R}$ and $\epsilon_i \in \mathbb{R}$, the representative model is then written as

$$y_i = f(x_i + \delta_i; \beta) - \epsilon_i, \quad i \in 1; \ldots; N, \tag{A.1}$$

where β are the parameters of the fitted model, and N the number of measurements. The ODR method consists of finding the parameter β that minimises the sum of orthogonal distances (that we label as r here) between the data points and the fit. The condition to be respected is

$$r = \min_{\beta,\delta,\epsilon} \frac{1}{2} \sum_{i=1}^{N} \left(\omega_{\delta_i} \delta_i^2 + \omega_{\epsilon_i} \epsilon_i^2 \right), \tag{A.2}$$

where $\omega_i = 1/\sigma_i^2$ is a weighting, introduced to compensate for instance when y_i and x_i have unequal precision. The final accuracy of the relation is deduced from the rms $\sigma_{\rm rms}$, that we compute in the following way:

$$\sigma_{\rm rms} = \sqrt{\frac{1}{N} \times \sum_{i=1}^{N} \left(F_{V_{\rm obs_i}} - F_{V_{\rm fit_i}} \right)^2}, \tag{A.3}$$

where $F_{V_{\rm obs_i}}$ is the measured surface brightness, and $F_{V_{\rm fit_i}}$ is the fit deduced from the ODR method introduced above. We then wanted to estimate the expected dispersion of surface brightnesses as a function of the $V-K$ colour of the star, according to our newly developed SBCR. Most authors compute the rms of the relation and plot a constant expected accuracy around their measurements. However, the weight of the measurements should be taken into account. Indeed, the number of measurements at a given colour indicates how precise the relation is. Following Gallenne et al. (2017), we searched for the barycentre of the measurements. To give clarity to our calculations, we note C as the $V-K$ colour. In this sense, the linear fit is written as follows:

$$F_V = a(C - C_0) + b, \tag{A.4}$$

where C_0 is the barycentre of the measurements. The extrapolated uncertainty on the model is then given by

$$\sigma_{F_V} = (C - C_0)^2 \sigma_a^2 + \sigma_b^2, \tag{A.5}$$

where σ_a and σ_b are, respectively, the uncertainties on the coefficient a and b of the fit. The condition to be satisfied here is finding C_0 so that $\rho = \partial r^2 / \partial a \partial b$ is zero, where r^2 is the distance between the fit and the data. The coefficient ρ corresponds to the correlation between a and b. With the previous condition, Eq. (A.5) becomes

$$\sigma_{F_V} = \sqrt{C^2 \sigma_a^2 + \sigma_b^2 + 2\rho\sigma_a\sigma_b C}. \tag{A.6}$$

For any dataset $(F_{V_i} \pm \sigma_i, C_i)$ and any value of C_0, the correlation ρ between a and b can be expressed as

$$\rho = -\frac{\partial^2 r^2 / \partial a \partial b}{\sqrt{(\partial^2 r^2 / \partial a^2)\,(\partial^2 r^2 / \partial b^2)}} = -\frac{\sum_i \frac{C_i - C_0}{\sigma_i^2}}{\sqrt{\sum_i \frac{(C_i - C_0)^2}{\sigma_i^2} \sum_i \frac{1}{\sigma_i^2}}}. \tag{A.7}$$

In order to simplify this equation into a more convenient form for estimating an order of magnitude, we made some basic assumptions. First, all the uncertainties σ_i on the surface brightness are equal, and then we assume $C_0 = 0$. In this particular case, Eq. (A.7) becomes

$$\rho = -\frac{\sum_i C_i}{\sqrt{N \sum_i C_i^2}}. \tag{A.8}$$

This method has the advantage of carefully estimating the extrapolated uncertainty of the linear model, depending on the number of measurements made at a given colour. This indicates that our SBCR will be more precise around the $V-K$ colour where most of the measurements were done.

Appendix B: VEGA visibility curves

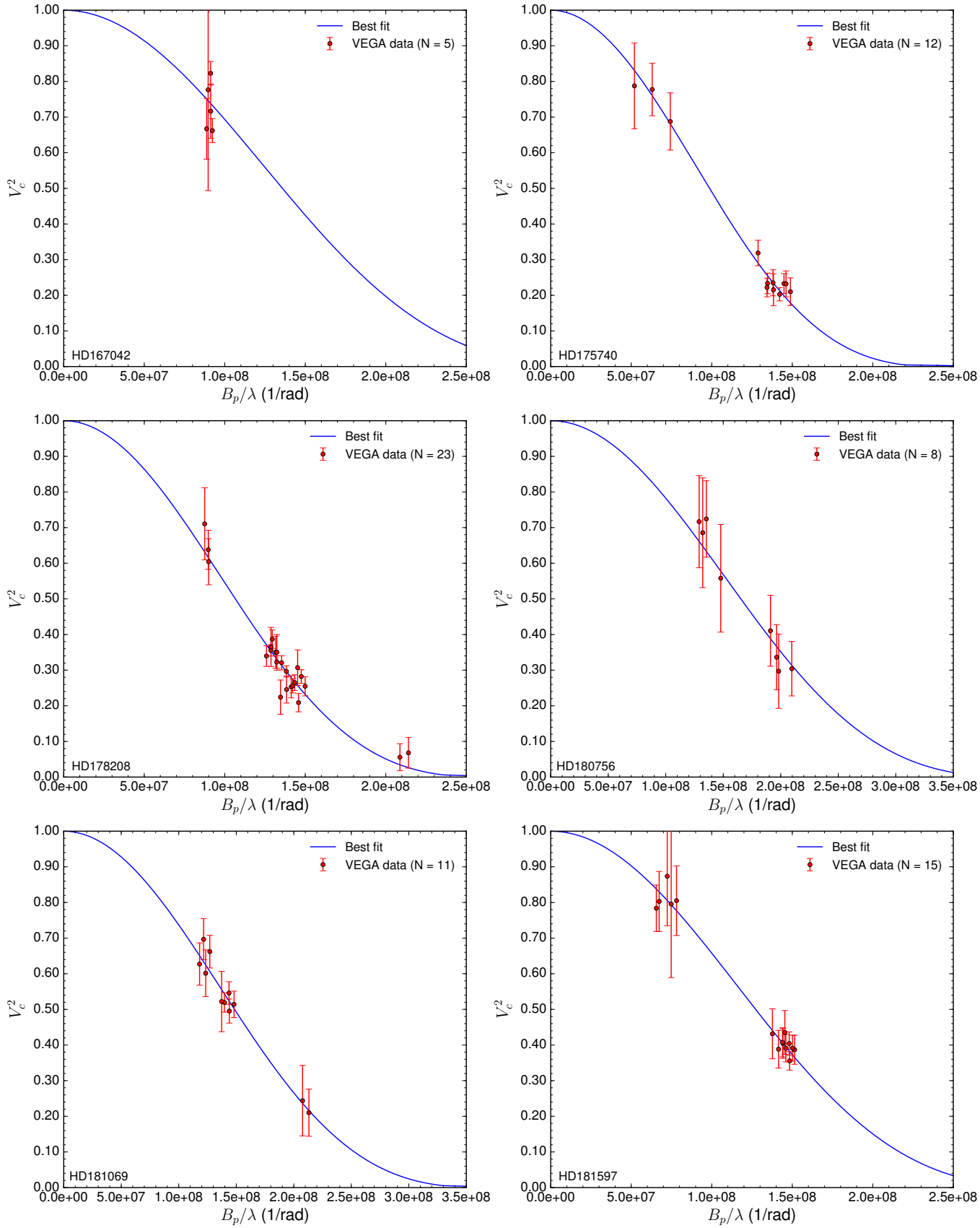

Fig. B.1. Interferometric squared visibilities of the ten benchmark stars measured by VEGA. The continuous line shows the best fitting model for a limb-darkened disc.

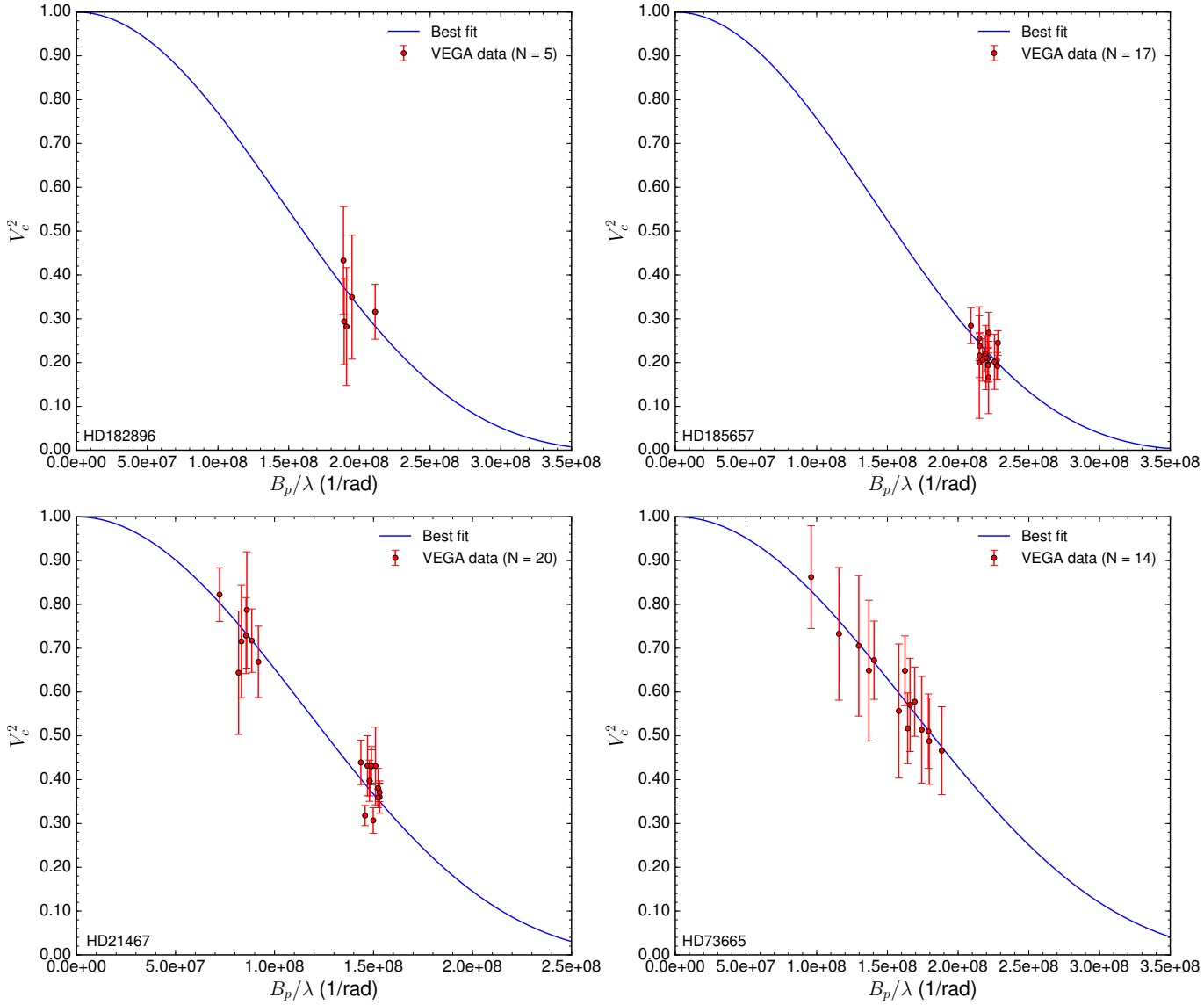

Fig. B.1. continued.

Table B.1. VEGA observing log.

Star	Date [yyyy.mm.dd]	Peak	AH [h]	λ [nm]	λ_{min} [nm]	λ_{max} [nm]	B_p [m]	Arg [deg]	SNR	$V^2_{cal_{\pm stat \pm syst}}$
HD 167042	2012.09.21	1	4.42	710	700	720	64.78	−179.01	24.90	$0.823_{\pm 0.033 \pm 0.001}$
	2012.09.22	1	2.32	710	700	720	65.55	−150.83	19.60	$0.662_{\pm 0.034 \pm 0.001}$
	2012.09.22	1	2.44	730	720	740	65.48	−152.38	2.75	$0.777_{\pm 0.283 \pm 0.001}$
	2013.07.29	1	4.77	710	700	720	64.81	176.13	9.39	$0.716_{\pm 0.076 \pm 0.001}$
	2013.07.29	1	4.77	730	720	740	64.81	176.16	7.82	$0.667_{\pm 0.085 \pm 0.001}$
HD 175740	2019.02.26	1	−5.08	710	700	720	36.93	−73.11	7.13	$0.788_{\pm 0.121 \pm 0.001}$
	2019.02.26	1	−4.29	710	700	720	44.76	−83.32	10.55	$0.777_{\pm 0.074 \pm 0.001}$
	2019.02.26	1	−3.36	710	700	720	52.73	−92.88	8.56	$0.688_{\pm 0.080 \pm 0.001}$
	2019.05.04	1	−2.41	730	720	740	94.01	−52.38	8.92	$0.319_{\pm 0.036 \pm 0.001}$
	2019.05.04	1	−1.90	730	720	740	98.05	−59.11	8.46	$0.222_{\pm 0.026 \pm 0.001}$
	2019.05.04	1	−1.52	730	720	740	100.78	−63.76	6.43	$0.235_{\pm 0.037 \pm 0.001}$
	2019.06.12	1	1.47	710	700	720	105.69	85.08	3.66	$0.210_{\pm 0.039 \pm 0.001}$
	2019.06.12	1	1.45	730	720	740	105.76	85.26	6.31	$0.232_{\pm 0.036 \pm 0.001}$
	2019.06.12	1	1.85	710	700	720	103.77	81.14	4.02	$0.233_{\pm 0.028 \pm 0.001}$
	2019.06.12	1	1.85	730	720	740	103.78	81.15	10.98	$0.203_{\pm 0.018 \pm 0.001}$
	2019.06.12	1	2.64	710	700	720	98.21	72.58	4.83	$0.216_{\pm 0.045 \pm 0.001}$
	2019.06.12	1	2.63	730	720	740	98.31	72.72	8.08	$0.233_{\pm 0.029 \pm 0.001}$
HD 178208	2017.03.13	1	−3.21	710	700	720	93.97	−37.00	7.00	$0.350_{\pm 0.050 \pm 0.001}$
	2017.03.13	1	−3.22	730	720	740	93.96	−36.97	6.66	$0.365_{\pm 0.055 \pm 0.001}$
	2017.04.12	1	−3.61	710	700	720	91.95	−30.63	7.74	$0.387_{\pm 0.026 \pm 0.001}$
	2017.04.12	1	−3.61	730	720	740	91.92	−30.54	6.79	$0.340_{\pm 0.029 \pm 0.001}$
	2017.04.12	1	−3.23	710	700	720	93.91	−36.83	6.46	$0.323_{\pm 0.017 \pm 0.001}$
	2017.04.12	1	−3.22	730	720	740	93.93	−36.88	7.11	$0.356_{\pm 0.016 \pm 0.001}$
	2017.04.12	1	−2.83	710	700	720	96.07	−42.87	6.41	$0.321_{\pm 0.020 \pm 0.001}$
	2017.04.12	1	−2.83	730	720	740	96.09	−42.92	7.01	$0.350_{\pm 0.045 \pm 0.001}$
	2017.04.12	1	−2.45	710	700	720	98.27	−48.60	4.91	$0.246_{\pm 0.038 \pm 0.001}$
	2017.04.12	1	−2.44	730	720	740	98.28	−48.64	4.49	$0.224_{\pm 0.048 \pm 0.001}$
	2017.04.12	1	−1.96	710	700	720	100.94	−55.38	5.12	$0.256_{\pm 0.020 \pm 0.001}$
	2017.04.12	1	−1.96	730	720	740	100.94	−55.38	5.93	$0.296_{\pm 0.016 \pm 0.001}$
	2017.04.12	1	−1.52	710	700	720	103.13	−61.16	6.21	$0.307_{\pm 0.050 \pm 0.001}$
	2017.04.12	1	−1.52	730	720	740	103.13	−61.17	5.06	$0.253_{\pm 0.031 \pm 0.001}$
	2017.04.12	1	−1.15	710	700	720	104.74	−65.83	5.64	$0.282_{\pm 0.019 \pm 0.002}$
	2017.04.12	1	−1.16	730	720	740	104.72	−65.78	5.25	$0.265_{\pm 0.022 \pm 0.001}$
	2017.04.12	1	−0.66	710	700	720	106.44	−71.87	5.10	$0.255_{\pm 0.027 \pm 0.001}$
	2017.04.12	1	−0.66	730	720	740	106.45	−71.90	4.15	$0.209_{\pm 0.026 \pm 0.001}$
	2017.07.28	1	2.73	710	700	720	152.00	30.73	1.36	$0.068_{\pm 0.043 \pm 0.001}$
	2017.07.28	1	2.73	728	718	738	152.00	30.73	1.11	$0.056_{\pm 0.038 \pm 0.001}$
	2017.09.16	1	4.72	710	700	720	63.73	−3.26	11.65	$0.638_{\pm 0.055 \pm 0.001}$
	2017.09.16	1	4.72	728	718	738	63.73	−3.25	7.02	$0.711_{\pm 0.101 \pm 0.001}$
	2017.09.16	1	5.22	710	700	720	63.89	−10.22	9.36	$0.604_{\pm 0.065 \pm 0.001}$
HD 180756	2017.06.21	1	−2.25	710	700	720	139.47	88.52	3.67	$0.336_{\pm 0.092 \pm 0.003}$
	2017.06.21	1	−2.25	730	720	740	139.47	88.52	4.12	$0.411_{\pm 0.100 \pm 0.004}$
	2017.06.21	1	−1.77	730	720	740	144.68	83.16	3.29	$0.297_{\pm 0.104 \pm 0.007}$
	2017.06.21	1	−1.31	710	700	720	148.81	78.04	3.98	$0.304_{\pm 0.076 \pm 0.002}$
	2017.05.13	1	−3.19	730	720	740	94.20	−37.30	5.76	$0.717_{\pm 0.129 \pm 0.001}$
	2017.05.13	1	−2.78	730	720	740	96.47	−43.66	4.45	$0.686_{\pm 0.154 \pm 0.001}$
	2017.05.13	1	−2.37	730	720	740	98.77	−49.64	6.75	$0.724_{\pm 0.107 \pm 0.001}$
	2017.05.13	1	0.37	730	720	740	107.91	−83.85	3.69	$0.558_{\pm 0.151 \pm 0.001}$
HD 181069	2017.04.15	1	−1.71	710	700	720	147.01	78.36	11.80	$0.244_{\pm 0.099 \pm 0.004}$
	2017.04.15	1	−1.29	710	700	720	150.93	74.72	11.56	$0.210_{\pm 0.066 \pm 0.003}$
	2017.04.15	2	−1.23	710	700	720	102.03	−67.84	17.15	$0.546_{\pm 0.032 \pm 0.007}$
	2017.04.15	2	−1.24	730	720	740	102.00	−67.79	19.07	$0.519_{\pm 0.027 \pm 0.006}$
	2017.04.15	2	−0.69	710	700	720	105.14	−73.62	13.87	$0.514_{\pm 0.037 \pm 0.007}$
	2017.04.15	2	−0.69	730	720	740	105.10	−73.55	14.70	$0.495_{\pm 0.034 \pm 0.006}$

Table B.1. continued.

Star	Date [yyyy.mm.dd]	Peak	AH [h]	λ [nm]	$\lambda_{\rm min}$ [nm]	$\lambda_{\rm max}$ [nm]	$B_{\rm p}$ [m]	Arg [deg]	SNR	$V^2_{\rm cal_{\pm stat \pm syst}}$
	2017.04.15	1	−3.09	710	700	720	86.35	−43.55	12.07	$0.697_{\pm 0.058 \pm 0.007}$
	2017.04.15	1	−3.10	730	720	740	86.23	−43.34	13.50	$0.627_{\pm 0.059 \pm 0.006}$
	2017.04.15	1	−2.67	710	700	720	90.17	−49.83	14.39	$0.662_{\pm 0.046 \pm 0.006}$
	2017.04.15	1	−2.68	730	720	740	90.11	−49.74	9.18	$0.601_{\pm 0.066 \pm 0.005}$
	2017.05.13	1	−1.49	730	720	740	100.23	−64.94	6.17	$0.522_{\pm 0.085 \pm 0.006}$
HD 181597	2019.03.14	1	−4.05	710	700	720	47.82	−78.30	8.64	$0.803_{\pm 0.084 \pm 0.001}$
	2019.03.14	1	−4.05	730	720	740	47.88	−78.41	10.36	$0.784_{\pm 0.065 \pm 0.001}$
	2019.03.14	1	−3.31	710	700	720	53.12	−87.57	3.80	$0.796_{\pm 0.206 \pm 0.001}$
	2019.03.14	1	−3.35	730	720	740	52.83	−87.06	6.29	$0.874_{\pm 0.139 \pm 0.001}$
	2019.03.14	1	−2.66	730	720	740	57.05	−94.84	8.23	$0.805_{\pm 0.098 \pm 0.001}$
	2019.05.04	1	−0.98	710	700	720	105.33	−68.00	13.70	$0.355_{\pm 0.026 \pm 0.001}$
	2019.05.04	1	−0.99	730	720	740	105.31	−67.92	9.69	$0.404_{\pm 0.042 \pm 0.001}$
	2019.05.04	1	−0.59	710	700	720	106.6	−72.77	10.69	$0.391_{\pm 0.037 \pm 0.001}$
	2019.05.04	1	−0.58	730	720	740	106.62	−72.85	10.16	$0.391_{\pm 0.038 \pm 0.001}$
	2019.05.04	1	−0.13	710	700	720	107.56	−78.12	9.48	$0.387_{\pm 0.041 \pm 0.001}$
	2019.06.15	1	1.69	710	700	720	105.14	80.90	12.33	$0.404_{\pm 0.033 \pm 0.001}$
	2019.06.15	1	1.71	730	720	740	105.07	80.69	9.98	$0.408_{\pm 0.041 \pm 0.001}$
	2019.06.15	1	2.11	710	700	720	103.23	75.97	7.06	$0.435_{\pm 0.062 \pm 0.001}$
	2019.06.15	1	2.10	730	720	740	103.28	76.08	7.37	$0.388_{\pm 0.053 \pm 0.001}$
	2019.06.15	1	2.58	730	720	740	100.51	70.10	6.14	$0.431_{\pm 0.070 \pm 0.001}$
HD 182896	2016.07.29	1	4.08	705	695	715	134.60	13.01	2.10	$0.282_{\pm 0.134 \pm 0.004}$
	2016.07.29	1	4.51	685	675	695	133.41	6.07	2.41	$0.349_{\pm 0.141 \pm 0.003}$
	2016.07.29	1	4.51	705	695	715	133.41	6.07	2.99	$0.294_{\pm 0.098 \pm 0.005}$
	2016.07.29	1	4.90	705	695	715	133.08	−0.38	3.52	$0.433_{\pm 0.123 \pm 0.010}$
	2016.08.21	1	2.44	685	675	695	144.64	36.85	5.04	$0.316_{\pm 0.063 \pm 0.006}$
HD 185657	2015.08.30	2	3.09	685	675	695	150.47	25.89	2.89	$0.212_{\pm 0.073 \pm 0.002}$
	2015.08.30	2	4.69	685	675	695	147.27	2.76	4.75	$0.255_{\pm 0.051 \pm 0.003}$
	2015.08.30	2	5.23	685	675	695	147.37	−5.32	4.26	$0.216_{\pm 0.050 \pm 0.002}$
	2015.08.30	2	5.24	705	695	715	147.37	−5.36	6.92	$0.284_{\pm 0.041 \pm 0.002}$
	2016.07.29	1	1.77	705	695	715	154.61	−136.84	5.36	$0.220_{\pm 0.041 \pm 0.001}$
	2016.07.29	1	1.77	685	675	695	154.61	−136.84	3.20	$0.202_{\pm 0.063 \pm 0.004}$
	2016.07.29	1	2.26	705	695	715	153.17	−143.03	4.26	$0.206_{\pm 0.048 \pm 0.005}$
	2016.07.29	1	2.75	685	675	695	151.56	−149.53	5.03	$0.194_{\pm 0.039 \pm 0.004}$
	2016.07.29	1	2.75	705	695	715	151.56	−149.53	1.57	$0.200_{\pm 0.127 \pm 0.003}$
	2016.08.21	1	1.22	685	675	695	155.80	−130.14	4.76	$0.206_{\pm 0.043 \pm 0.001}$
	2016.08.21	1	1.22	705	695	715	155.80	−130.14	4.18	$0.209_{\pm 0.050 \pm 0.001}$
	2016.08.21	1	2.70	685	675	695	151.74	−148.81	2.01	$0.166_{\pm 0.082 \pm 0.004}$
	2016.08.21	1	2.70	705	695	715	151.74	−148.81	7.91	$0.238_{\pm 0.030 \pm 0.005}$
	2016.10.01	1	0.65	685	675	695	156.27	−123.49	8.62	$0.245_{\pm 0.028 \pm 0.001}$
	2016.10.01	1	0.63	705	695	715	156.27	−123.26	5.78	$0.268_{\pm 0.046 \pm 0.001}$
	2016.10.01	1	1.07	685	675	695	156.01	−128.29	6.19	$0.192_{\pm 0.031 \pm 0.001}$
	2016.10.01	1	1.05	705	695	715	156.04	−128.13	4.97	$0.196_{\pm 0.039 \pm 0.001}$
HD 21467	2017.09.17	1	−0.54	705	695	715	104.22	−78.86	8.61	$0.430_{\pm 0.038 \pm 0.001}$
	2017.09.17	1	−0.56	725	715	735	104.11	−78.75	8.67	$0.439_{\pm 0.051 \pm 0.001}$
	2017.09.17	1	−0.11	725	715	735	106.54	−81.58	6.30	$0.432_{\pm 0.068 \pm 0.001}$
	2017.09.17	1	0.57	705	695	715	107.91	−85.64	7.20	$0.360_{\pm 0.037 \pm 0.001}$
	2017.09.17	1	0.57	725	715	735	107.92	−85.62	8.62	$0.431_{\pm 0.089 \pm 0.001}$
	2017.09.17	1	0.97	705	695	715	107.40	−87.91	7.61	$0.381_{\pm 0.045 \pm 0.001}$
	2017.09.17	1	0.97	725	715	735	107.39	−87.93	7.93	$0.397_{\pm 0.047 \pm 0.001}$
	2017.10.13	1	0.15	705	695	715	64.73	−123.49	8.22	$0.669_{\pm 0.081 \pm 0.001}$
	2017.10.13	1	0.87	705	695	715	62.39	−129.25	9.93	$0.717_{\pm 0.072 \pm 0.001}$
	2017.10.13	1	0.88	725	715	735	62.34	−129.35	5.93	$0.787_{\pm 0.133 \pm 0.001}$
	2017.10.13	1	1.35	705	695	715	60.35	−133.68	8.41	$0.729_{\pm 0.087 \pm 0.001}$
	2017.10.13	1	1.34	725	715	735	60.36	−133.66	5.57	$0.715_{\pm 0.128 \pm 0.001}$
	2017.10.17	1	−0.30	705	695	715	105.65	−80.40	6.14	$0.307_{\pm 0.029 \pm 0.001}$

Table B.1. continued.

Star	Date [yyyy.mm.dd]	Peak	AH [h]	λ [nm]	$\lambda_{\min}$ [nm]	$\lambda_{\max}$ [nm]	B_p [m]	Arg [deg]	SNR	$V^2_{\mathrm{cal}_{\pm\mathrm{stat}\pm\mathrm{syst}}}$
	2017.10.17	1	−0.30	725	715	735	105.66	−80.41	6.36	$0.318_{\pm0.023\pm0.001}$
	2017.10.17	1	0.11	705	695	715	107.29	−82.91	7.19	$0.359_{\pm0.019\pm0.001}$
	2017.10.17	1	0.11	725	715	735	107.29	−82.91	7.95	$0.397_{\pm0.034\pm0.001}$
	2017.10.17	1	0.52	705	695	715	107.91	−85.32	7.42	$0.371_{\pm0.021\pm0.001}$
	2017.10.17	1	0.52	725	715	735	107.91	−85.32	8.63	$0.432_{\pm0.044\pm0.001}$
	2017.12.09	1	1.89	705	695	715	57.70	−139.60	4.57	$0.644_{\pm0.141\pm0.008}$
	2017.12.10	1	−3.64	725	715	735	52.36	−105.26	13.41	$0.822_{\pm0.061\pm0.005}$
HD 73665	2018.04.26	1	2.51	705	695	715	126.21	−137.82	6.02	$0.511_{\pm0.085\pm0.004}$
	2018.04.26	1	2.96	705	695	715	119.37	−144.11	7.31	$0.578_{\pm0.079\pm0.005}$
	2018.04.26	1	2.98	725	715	735	119.14	35.67	6.40	$0.517_{\pm0.081\pm0.004}$
	2018.10.21	1	−5.69	710	700	720	68.22	171.29	7.35	$0.862_{\pm0.117\pm0.001}$
	2018.10.21	1	−8.63	710	700	720	82.18	84.62	4.84	$0.733_{\pm0.151\pm0.002}$
	2018.10.21	1	−1.49	730	720	740	94.72	106.58	4.40	$0.705_{\pm0.160\pm0.001}$
	2018.10.21	1	−1.03	710	700	720	99.82	−76.59	7.54	$0.673_{\pm0.089\pm0.002}$
	2018.10.21	1	−1.02	730	720	740	99.95	103.32	4.04	$0.649_{\pm0.161\pm0.001}$
	2018.12.16	1	2.00	710	700	720	133.79	48.08	4.65	$0.466_{\pm0.100\pm0.004}$
	2018.12.16	1	2.42	710	700	720	127.50	43.24	4.95	$0.488_{\pm0.099\pm0.004}$
	2018.12.16	1	2.44	730	720	740	127.22	43.02	4.22	$0.514_{\pm0.122\pm0.003}$
	2018.12.16	1	2.84	730	720	740	121.16	37.67	8.05	$0.571_{\pm0.106\pm0.004}$
	2018.12.16	1	3.25	710	700	720	115.30	31.43	5.85	$0.648_{\pm0.080\pm0.006}$
	2018.12.16	1	3.24	730	720	740	115.40	31.55	5.27	$0.557_{\pm0.153\pm0.004}$